Environmental Science & Technology

Article

pubs.acs.org/est

Global Intraurban Intake Fractions for Primary Air Pollutants from Vehicles and Other Distributed Sources

Joshua S. Apte,[†] Emilie Bombrun,[‡] Julian D. Marshall,*[,‡] and William W. Nazaroff[§]

[†]Energy and Resources Group, University of California, Berkeley, California 94720-3050, United States

[‡]Department of Civil Engineering, University of Minnesota, Minneapolis, Minnesota 55455-0233, United States

[§]Department of Civil and Environmental Engineering, University of California, Berkeley, California 94720-1710, United States

Supporting Information

ABSTRACT: We model intraurban intake fraction (iF) values for distributed ground-level emissions in all 3646 global cities with more than 100 000 inhabitants, encompassing a total population of 2.0 billion. For conserved primary pollutants, population-weighted median, mean, and interquartile range iF values are 26, 39, and 14−52 ppm, respectively, where 1 ppm signifies 1 g inhaled/t emitted. The global mean urban iF reported here is roughly twice as large as previous estimates for cities in the United States and Europe. Intake fractions vary among cities owing to differences in population size, population density, and meteorology. Sorting by size, population-weighted mean iF values are 65, 35, and 15 ppm, respectively, for cities with populations larger than 3, 0.6−3, and 0.1−0.6 million. The 20 worldwide megacities (each >10 million people) have a population-weighted mean iF of 83 ppm. Mean intraurban iF values are greatest in Asia and lowest in land-rich high-income regions. Country-average iF values vary by a factor of 3 among the 10 nations with the largest urban populations.

1. INTRODUCTION

Air pollution exposure is associated with adverse health effects.[1−4] Efforts to improve air quality focus on reducing emissions. Air quality management includes deciding which sources to control and by how much. Intake fraction estimates could help guide such prioritization efforts.

Intake fraction (iF) summarizes the emission-to-intake relationship for a specific source as the fraction of emissions that are inhaled by an exposed population.[5] Intake fraction can be used in cost-benefit and cost-effectiveness analyses, investigations of environmental equity, health risk assessment, and other studies that estimate the exposure consequences of emissions.[6−8]

Intake fraction varies spatially and temporally, depending on factors such as the size of the exposed population, proximity between people and emissions, and environmental persistence of a pollutant. Reported iF values for nonreactive motor vehicle emissions include the following results: 0.1−0.5 ppm for U.S. rural areas,[9] 3−21 ppm for U.S. cities of typical size,[10,11] and 29−280 ppm for three global megacities (Los Angeles,[12] Mexico City,[13] and Hong Kong[14]). An iF of 10 ppm (i.e., 10^{-5}) means that an exposed population inhales an aggregate increment of 10 grams per tonne emitted. Prior investigations of iF for urban vehicle emissions have emphasized conditions for North America and Europe; determinants such as meteorology and urban form may differ on other continents. Moreover, vehicle use is increasing rapidly in countries such as China and India for which few iF estimates exist.[15−19]

Here, we use a modeling approach to estimate intraurban iF values for distributed ground-level primary pollutant emissions for all worldwide cities with a year 2000 population of 100 000 or more. In aggregate, this set of 3646 cities contains 2.0 billion people (for year 2000), including ∼1 billion people in Asia. A goal of this study is to elucidate global patterns of intraurban iF among countries, regions, and cities of varying sizes. We extend a previously published approach for estimating iF,[13] incorporating global data sets of demographic and meteorological parameters as model inputs. Our investigation is motivated by trying to better understand the exposure consequences of urban vehicle emissions. The results may be informative for any broadly distributed source of ground-level emissions to outdoor urban air.

Received: November 11, 2011
Revised: February 2, 2012
Accepted: February 14, 2012
Published: February 14, 2012

2. METHODS

2.1. Intake Fraction. The intake fraction for atmospheric emissions can be evaluated as

$$\text{intake fraction} = \frac{\text{population intake}}{\text{total emissions}} = \frac{\int_{T_1}^{\infty}\left(\sum_{i=1}^{P}\left(C_i(t)Q_i(t)\right)\right)\mathrm{d}t}{\int_{T_1}^{T_2}E(t)\mathrm{d}t} \quad (1)$$

where T_1 and T_2 are the starting and ending times of emissions, P is the number of people exposed, $Q_i(t)$ is the volumetric breathing rate ($m^3\ s^{-1}$) for individual i at time t, $C_i(t)$ is the incremental concentration ($g\ m^{-3}$) at time t in individual i's breathing zone that is attributable to the emissions, and $E(t)$ is the emission rate ($g\ s^{-1}$) at time t.[12] The integrals in eq 1 are evaluated numerically, as detailed below.

2.2. Emissions−Exposure Concentration Relationship. *2.2.1. Model Selection.* Intake fractions depend on the relationship between emissions and exposure concentrations. Previous studies have employed various methods with differing levels of complexity and data requirements. Examples include one-compartment Eulerian models,[8,10,11] Gaussian plume models,[20,21] coarse-grid Eulerian models,[13,22] empirical estimates using tracers of opportunity,[12,13,23,24] and intentional tracer-gas experiments.[25]

In this paper, we designate urban areas with a population of at least 100 000 as "cities". For the large number of cities considered here, an efficient approach is needed that can provide good estimates with a reasonable level of effort per city. We consider spatially distributed ground-level emissions sources (e.g., vehicles) and use a one-compartment Eulerian model. We estimate the intraurban iF for each city, i.e., the iF associated with residents' inhalation of emissions from their city.

Compared to alternatives, there are several advantages of the one-compartment Eulerian model: (1) Input data are available globally using uniform methods. (2) Studies comparing iF estimated using this model have found similar results compared with studies using empirical data or complex air-dispersion models.[11,12] (3) Because this type of model is widely used,[26−28] the results reported here can be directly applied as model input parameters. (4) The one-compartment model is readily scaled in size for each location studied. Among the limitations of this approach are that (1) the model excludes within-urban variability, (2) we have not evaluated iF for secondary pollutants or for nonconserved species with other than first-order decay, and (3) as applied here, we only consider intraurban exposures. Previous findings suggest that for estimating iF for individual cities, this approach is accurate within a factor of ∼2 or better for primary pollutants.[11−13] We judge this accuracy to be acceptable given the efficiency of the approach; global intraurban iF values reported here vary by much more than a factor of 2.

2.2.2. One-Compartment Emissions−Concentration Model. The following equation, derived from mass balance, embodies a dynamic one-compartment model for predicting a primary-pollutant concentration increment resulting from emissions:[13,29]

$$\frac{\mathrm{d}C(t)}{\mathrm{d}t} = \frac{E(t)}{LWH(t)} - C(t)\left(k + \frac{u(t)}{L} + \phi\frac{1}{H(t)}\frac{\mathrm{d}H}{\mathrm{d}t}\right) \quad (2)$$

Here, $C(t)$ is the incremental concentration attributable to the emissions source ($g\ m^{-3}$), which varies with time, t (s), $E(t)$ is the emission rate from the source under consideration ($g\ s^{-1}$), L and W are the windward and crosswind dimensions, respectively (m), of the model domain, $H(t)$ is the atmospheric mixing height (m), k is the first-order decay constant (s^{-1}), and $u(t)$ is the wind speed averaged over the mixing height ($m\ s^{-1}$). The parameter ϕ accounts for dilution of contaminated urban air by clean air aloft during periods of increasing mixing height as follows: $\phi = 0$ when $\mathrm{d}H/\mathrm{d}t$ is nonpositive (H decreasing or constant), and $\phi = 1$ when $\mathrm{d}H/\mathrm{d}t$ is positive (H increasing). Stevens et al.[13] were the first to apply this dynamic model to estimate urban iF; eq 2 extends their approach to incorporate pollutants that undergo first-order decay with rate constant k. Base-case iF analyses are presented in this paper for conserved, nonreactive emissions ($k = 0$). Many important vehicle-emitted species—such as carbon monoxide (CO), benzene, and primary (i.e., directly emitted) constituents of fine particulate matter ($PM_{2.5}$), including black carbon particles—are reasonably modeled as conserved within urban areas, since $k \ll u/L$. Sensitivity cases are simulated for decaying pollutants with 10 and 100 h half-lives (k = 1.7 and 0.17 d^{-1}, respectively). Example species in these classes are acetaldehyde and toluene (∼10 h half-life) and methyl *tert*-butyl ether (MTBE; ∼100 h half-life).[30] For the primary pollutants considered here, the iF is independent of the time-averaged emissions rate.[6] Likewise, the intraurban primary-pollutant iF for any source is, by definition, independent of background concentrations imposed by other sources and by regional transport. Consequently, city-specific emissions and concentration data are not required as model inputs.

In implementation, eq 2 is converted from differential to finite-difference form, and the model simulates a series of time steps. We use short time steps: 7.5 min for a 3 year simulation of each urban area. We assumed a constant annual-average emission rate for all cities in our data set and specified initial and upwind boundary conditions for each city as $C = 0$. We tested the numerical integration to ensure it behaves as expected for these conditions: (1) in simple scenarios with known outcome (e.g., step change for one input parameter) and (2) by matching inputs and outputs from Stevens et al.[13] Discretization errors resulting from numerical integration of eq 2 are estimated to be less than 1%.

2.3. Model Input Data. *2.3.1. Meteorological Data.* We acquired location-specific and time-resolved mixing heights and wind speeds for the years 2007−2009 from NASA's Modern-Era Retrospective Analysis for Research and Applications (MERRA).[31] MERRA uses the Goddard Earth Observing System (GEOS) atmospheric model to assimilate historical meteorological and climatological observations into a global data set with high spatiotemporal resolution (1/2° longitude × 2/3° latitude × 1 h; in the middle latitudes, these values correspond to a spatial resolution of ∼56 × 74 km). Each city in our data set was matched to the nearest MERRA grid point. The median distance between the centroid of each city's urbanized land area and the corresponding MERRA grid point was 23 km (10% trimmed range 10−34 km).

MERRA data provide the wind speed at a standard 10 m reference height. To obtain the mixing-height-averaged wind speed, we employed a truncated power-law relationship for wind speed versus height (see the Supporting Information).[13,29] We used literature-recommended values for the vertical interpolation of wind speed as default input parameters and considered alternate values in sensitivity analyses (see the Supporting Information).[29,32,33]

2.3.2. Breathing Rate. Volumetric breathing rates for populations follow diurnal patterns, owing to variations in the levels of physical activity and in physiological processes (e.g., circadian rhythm).[34−36] Few data sets are available to characterize the temporal pattern of breathing rate for large urban populations. Here, we developed a diurnal profile using time-activity data from a large probability-based sample of the U.S. population[37] and activity-dependent inhalation rates (see the Supporting Information).[35,36] Relative to the time-integrated mean, the diurnal profile varies from 47% lower (03:00 to 04:00 h) to 33% higher (at 15:00 h) (see the Supporting Information). For base-case and sensitivity analyses, the time-integrated mean breathing rate was taken to be 14.5 m^3 $person^{-1}$ d^{-1}, consistent with long-term average inhalation rates recommended by the U.S. Environmental Protection Agency (USEPA).[35] This metabolically derived value is comparable to those used in other recent iF analyses (range 13−14.5 m^3 $person^{-1}$ d^{-1}),[8,14,24] and lower than the upper-bound breathing rate value of 20 m^3 $person^{-1}$ d^{-1} employed in some studies.[9,13] To test the sensitivity of the results to the inferred time pattern of population breathing, we considered four alternative patterns: constant, a sinusoidal daily cycle[34] (amplitude ± 25% of the mean), and two previously published profiles for the United States (Figure SI.4, Supporting Information).[11,38]

2.3.3. Data for Each Urban Area. We estimated intake fractions for the 3646 worldwide urban areas that had at least 100 000 inhabitants in the year 2000 utilizing a data set compiled by Angel et al.[39,40] The total population in this data set (2.0 billion) accounts for 71% of the total year 2000 global urban population and 32% of the global population.[40] The following information is available for each city: population, land area (A, km^2, derived from satellite data),[41] and location (latitude and longitude). In cases where a contiguous urbanized area spans several administrative units (e.g., for "conurbations" or "urban agglomerations"), this database generally provides a single population and land area estimate for the urban portion of the entire metropolitan region. To our knowledge, this database contains the most consistent and comprehensive global set of urban population and land area data available.[42] We idealize each city as occupying a square-plan urban footprint ($L = W = A^{0.5}$) and consider variations in the aspect ratio, $\alpha = L/W$, as a sensitivity parameter.

2.3.4. Emissions Profile. Since concentrations of primary nonreactive or first-order decaying pollutants scale linearly with emissions, intake fractions are independent of emission rates that are constant. However, because breathing rates and meteorology vary systematically, diurnal emission rate patterns can influence the intake fraction. For base-case analyses, we developed an "archetypal" diurnal emissions profile based on mobile source emission inventories for Beijing, China,[43] Mexico City, Mexico,[13] and New Delhi, India[44] (see the Supporting Information). The sensitivity of the results to the choice of diurnal emissions profile was tested using the following alternatives: (a) time-invariant emissions, (b) individual diurnal profiles from each of the three above cities, and (c) emissions scaled to diurnal vehicle activity data (vehicle km h^{-1}) from the USEPA National Emissions Inventory (Figure SI.5, Supporting Information).[45] Each simulation utilized a single diurnal profile. (We did not account for weekday−weekend differences in the timing of emissions or breathing rates.)

2.4. Steady-State Intake Fraction. As a complement to the time-dependent numerical solution described above, we illustrate here an approximate analytical solution that aids in conceptual interpretation of the results. Substituting the steady-state solution for eq 2 into eq 1 yields the following relationship for the iF of a conserved species in a square-plan urban area:[6,10,11]

$$\mathrm{iF} \approx \bar{Q}_i(P/\sqrt{A})(\overline{1/uH}) = \bar{Q}_i(\mathrm{LPD})(\mathrm{DR})^{-1} \approx \frac{\text{population breathing rate}}{\text{urban ventilation rate}} \quad (3)$$

This relationship can be decomposed into three parameter groups that provide insight into the key drivers of iF.[11] The first term, $\bar{Q}_i$, is the time-averaged per-capita mean breathing rate (m^3 s^{-1} $person^{-1}$). The second group, linear population density (LPD = $P/\sqrt{A}$, persons m^{-1}), is a property of a city's urban form that represents the mean population per unit length (in the windward direction) of urbanized land.[11,46] The final parameter group, normalized dilution rate (DR = $(\overline{1/uH})^{-1}$), characterizes atmospheric dilution (wind speed times mixing height, m^2 s^{-1}).[11] For each city, we compute DR as the long-term harmonic mean of the product of linearly interpolated hourly values of u and H. The ratio DR/LPD can be intuitively understood as an effective per-capita atmospheric dilution rate available for an urban area. The intraurban intake fraction is proportional to the ratio of the population breathing rate to this per-capita atmospheric dilution rate (iF ≈ $\bar{Q}_i$[DR/LPD]$^{-1}$).

3. RESULTS AND DISCUSSION

3.1. Global and Regional Intake Fraction Summary. Table 1 presents summary metrics of population-weighted and unweighted distributions of iF values. Among all cities, the population-weighted mean intraurban iF for distributed ground-level emissions of conserved pollutants is 39 ppm (IQR = 14−52 ppm). Population-weighted results are computed by weighting each city's iF by its population (i.e., equal weight per person), whereas unweighted results treat each city as a distinct

Table 1. Global Summary of Intraurban Intake Fraction, Demographic Parameters, and Meteorology[a,b]

	intake fraction (ppm)		population (millions)		LPD (persons m^{-1})		DR (m^2 s^{-1})	
range of values	0.6−260		0.1−34		5.8−780		32−10000	
AM (ASD)	39 (36)	*17 (18)*	4.2 (6.4)	*0.55 (1.4)*	170 (150)	*59 (58)*	540 (460)	*520 (460)*
GM (GSD)	26 (2.5)	*12 (2.2)*	1.5 (4.7)	*0.28 (2.6)*	110 (2.5)	*45 (2.0)*	470 (1.6)	*450 (1.6)*
median	26	*12*	1.4	*0.21*	110	*41*	450	*430*
IQR	14−52	*7.3−20*	0.42−5	*0.13−0.43*	57−220	*28−67*	370−550	*360−530*
$P_{10} - P_{90}$	7.7−80	*4.7−34*	0.18−13	*0.11−1.1*	33−370	*20−110*	300−770	*300−750*

[a]Nonitalicized entries (left column under each column head) reflect population-weighted statistics; italicized entries (right column under each column head) are unweighted results. [b]Abbreviations: LPD, linear population density; DR, normalized dilution rate; AM, arithmetic mean; ASD, arithmetic standard deviation; GM, geometric mean; GSD, geometric standard deviation; IQR, interquartile range; P_{10} and P_{90}, 10th and 90th percentiles of distribution.

unit with equal weight.[11] Because iF is correlated with population, weighted metrics better reflect the distribution of iF over the global population of city inhabitants. For the remainder of this paper, we employ population-weighted metrics of iF unless stated otherwise. All reported results reflect the full numerical solution to the iF model as outlined in section 2.2.

Intake fraction varies over almost 3 orders of magnitude among all cities (full range 0.6−260 ppm, 10% trimmed range 7.7−80 ppm). The population-weighted distribution of iF conforms well to a log-normal form (geometric mean (GM) 26 ppm, geometric standard deviation (GSD) 2.5, Figure SI.6, Supporting Information). Respectively 530, 260, and 120 million people live in cities with iF values greater than 50, 75, and 100 ppm.

3.1.1. Reduced-Form Intake Fraction Model. Variation in iF among cities is predicted well by a parsimonious regression model using the following three-parameter fit:

$$\mathrm{iF} = (74.0\ \mathrm{ppm})(\mathrm{LPD})^{0.980}(\mathrm{DR})^{-0.876}A^{-0.0497} \quad (4)$$

where units on the parameters are as specified in section 2.4. This regression can be used with reasonable accuracy to rapidly estimate iF for any city in the global data set (r^2 = 0.99, root-mean-square prediction error 9%). In addition, the reduced-form model provides a framework for understanding how variation in iF is governed by urban form and meteorology. Globally, LPD is more variable than DR (interquartile ranges are 57−220 persons m^{-1} for LPD and 370−550 m^2 s^{-1} for DR). Holding other variables constant, an IQR increase in linear population density results in a 3.8-fold increase in iF, while an IQR reduction in normalized dilution rate results in only a 42% increase in iF.

3.1.2. Patterns of Intake Fraction by City Size, World Region, and Country. Larger cities tend to have higher iF values (Figure 1). To illustrate, we divide the city data set into three population-based groupings of nearly equal total population: small cities with between 100 000 and 600 000 inhabitants (32% of the total city population), medium cities with 600 000 to 3 million inhabitants (34%), and large cities with >3 million inhabitants (34%). Population-weighted mean intraurban iF values for these three groupings are, respectively, 15, 35, and 65 ppm. Variation in iF by city size is principally attributable to the strong correlation between LPD and urban population. On average, each 1% increase in city population is associated with a 0.57% increase in LPD (r^2 = 0.62). Interestingly, LPD is much more variable among the three different city size groupings than is population density (mean LPD = 50, 130, and 310 persons m^{-1}, mean density = 110, 150, and 120 persons m^{-2}). The DR is uncorrelated with the population (r^2 = 0.013).

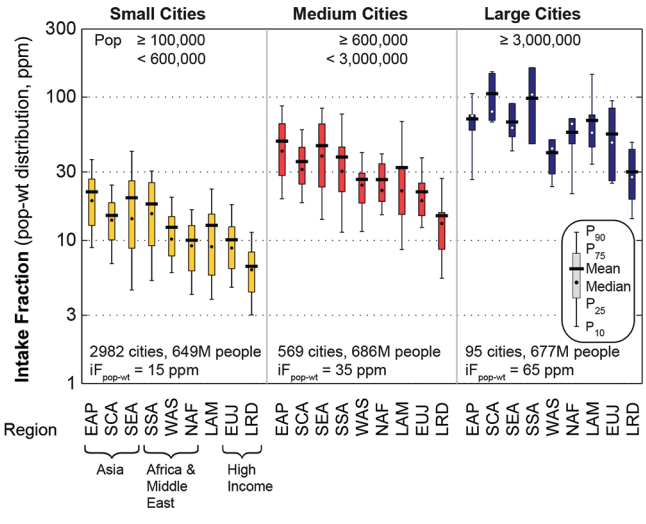

Figure 1. Population-weighted distribution of intraurban intake fraction by city size (small, medium, large) and region (labels on horizontal axis; see Table 2 and the map in Figure SI.7 (Supporting Information) for definitions of the abbreviations). For cities of similar size, iF is generally higher in Asia (e.g., EAP, SCA, and SEA) and lower in high-income regions (e.g., EUJ and LRD). See Table SI.3 (Supporting Information) for a tabulation of the results.

Intake fractions differ substantially among geographic regions (Table 2, Figures 1 and 2). Following Angel et al.,[39,40] we group the world into nine clusters that reflect varying land-use patterns (Figure SI.7, Supporting Information). Among these regions, mean intraurban iF varies by a factor of 2.7 (Table 2). Regions with especially high mean intraurban iF values include South and Central Asia (SCA; mean 55 ppm), Southeast Asia (SEA; 48 ppm), East Asia and the Pacific (EAP; 44 ppm), and sub-Saharan Africa (SSA; 43 ppm). By contrast, iF is comparatively low for land-rich developed countries (LRD; 20 ppm). Comparing Asia with North and Central America highlights regional properties of urban settlement (Figure 2). The Asian cities mapped in Figure 2 have a high mean intraurban iF (48 ppm) and a large total population (914 million, ~45% of all global city inhabitants). Of all cities with intraurban iF ≥ 100 ppm (n = 24 cities), 75% (n = 18) are in Asia and 50% (n = 12) are in China.

Regional patterns of iF are independent of city size, such that similar trends in iF emerge within each of the small, medium, and large city groupings (Figure 1). As a result, iF values for smaller cities in some regions may be greater than those for more populous cities elsewhere. For example, the mean iF for small cities in EAP (22 ppm) is greater than that for medium cities in LRD (15 ppm).

Country-average intraurban iF varies by more than a factor of 3 among the 10 countries with the largest urban populations (Table 3; Table SI.9, Supporting Information). Mean intraurban iF values in Mexico (65 ppm), Indonesia (53 ppm), India (51 ppm), and China (44 ppm) are greater than in Australia (14 ppm), the United States (21 ppm), Germany (30 ppm), and Russia (32 ppm).

Regional variation in iF is attributable to urban form and meteorology (Table 2). For example, the high mean iF value in South and Central Asia (41% greater than the global mean) is attributable to high LPD (37% greater than the global mean) and weaker-than-average dilution (DR 9% below the global mean). Similarly, relatively low iF in land-rich developed countries (47% lower than the global mean) is explained by low LPD (36% lower than the global mean) and more favorable atmospheric dilution (DR 11% greater than the global mean). The range in LPD among the nine regions is roughly twice as large as the range for DR (Table 2). However, local patterns in wind speed and mixing height give rise to apparent "hotspots" where meteorology has a more pronounced role influencing iF. For example, DR is ~30−60% lower than the global average in the Indo-Gangetic Plain (Pakistan, northern India, Bangladesh) and in heavily forested equatorial regions (Amazon and Congo River basins, parts of Indonesia). Globally, spatial variation in long-term DR depends more on the variation in wind speed than on the variation in mixing height.

3.1.3. Megacities. The air quality challenge of megacities (population >10 million) has received considerable attention.[47−55]

Table 2. Regional Summary of Intraurban Intake Fraction, Population Density, and Meteorology[a]

region		iF (ppm)	LPD (persons m^{-1})	density (persons ha^{-1})	DR (m^2 s^{-1})	city population (millions)	N (cities)
SCA	South and Central Asia	55	230	160	490	290	539
SEA	Southeast Asia	48	170	120	520	110	196
EAP	East Asia and Pacific	44	180	220	480	460	891
SSA	sub-Saharan Africa	43	160	170	610	130	258
LAM	Latin America	41	170	87	610	260	403
NAF	North Africa	32	180	130	630	53	115
EUJ	Europe and Japan	30	140	59	530	400	796
WAS	Western Asia	26	120	91	550	90	157
LRD	land-rich developed	20	110	29	600	230	291

[a]Population-weighted arithmetic means for cities with populations ≥100 000. Total population 2.0 billion people (72% of the year 2000 urban population, 32% of the global population) in 3646 cities.

Table 3. Population-Weighted Mean Intraurban Intake Fraction for the 10 Countries with the Largest Population in Cities[a]

country	iF (ppm)	city population (millions)	country	iF (ppm)	city population (millions)
China	44	412	Mexico	65	58
United States	21	192	Germany	30	49
India	51	188	Indonesia	53	40
Brazil	33	88	South Korea	46	36
Japan	50	85	all 10 countries	41	1216
Russia	32	68	other 148 countries	35	796

[a]The cities considered are all urban areas with populations ≥100 000.

The 20 megacities in this data set account for ~15% of the total city population (300 million people) and have a population-weighted mean iF of 83 ppm (IQR = 48−94 ppm, range 25−260 ppm). Four megacities have intake fractions that exceed 100 ppm: New Delhi, India; Kolkata, India; Dhaka, Bangladesh; and Mexico City, Mexico (Figure 2; Table SI.8, Supporting Information). Although the overall population density for megacities is nearly the same as the global mean for cities of all sizes (mean 125 persons ha^{-1}), the LPD in megacities is 2.5 times the global urban average (410 [megacities] versus 170 [global average], persons m^{-1}) owing to megacities' large spatial extent (mean area 2300 km^2).

The total intraurban population intake ($E \times$ iF) of emissions in megacities may be especially high. Megacities have been identified elsewhere as emissions hotspots.[48,50,52] High iF in megacities magnifies the exposure relevance of these emissions. For example, consider a hypothetical pollutant emitted on an equal per-capita basis everywhere. For that pollutant, a city's total intraurban intake would scale with the product of population and iF. Under such conditions, the world's 20 megacities would themselves account for 32% of the global intraurban intake or more than double the 15% of the global city population that they contain.

3.1.4. Time of Day and Seasonal Patterns in iF. Diurnal trends in atmospheric mixing and population breathing rate lead to variability in iF as a function of emissions timing. In general, iF is elevated for emissions that occur during periods of weak atmospheric dispersion (e.g., nighttime, Figure SI.8, Supporting Information). Considering all cities, the median iF for emissions at night (21:00 to 03:00 h) is 8.5 times greater (IQR = 5.1−11 times) than for emissions during the day (09:00 to 15:00 h). The strong role of atmospheric mixing in driving nighttime maxima in iF is highlighted when considering that our model accounts for higher-than-average population breathing rates during daytime hours. Interestingly, diurnal cycles in mixing height are principally responsible for the temporal pattern in a city's short-term DR, in contrast to the observation above that regional variation in long-term DR is primarily attributable to between-city differences in mean wind speed.

Compared to diurnal variability, monthly differences in iF are less pronounced. The median ratio of maximum to minimum month-averaged iF among all cities is 2.3 (IQR = 1.8−2.9). On average, iF values in nontropical cities are 13 times greater (IQR = 9.1−15 times) during winter nights than summer days. Interannual variability in meteorology for the 3 years considered in this study (2007−2009) has a negligible (<1%) effect on global mean iF and also little effect on iF values for individual cities (10% trimmed range ~±5%).

3.2. Validation and Comparison with Prior Research. Several previous studies have estimated iF values of urban vehicle emissions for individual cities, countries, or regions, principally in North America and Europe. For large groups of cities with diverse population sizes, prior estimates of population-weighted average iF values for vehicle emissions are in the range of ~5−20 ppm,[9,11,22,56] with higher iF values reported for individual large cities (e.g., Mexico City, Hong Kong, Los Angeles).[12−14,23] The higher population-weighed mean iF result obtained here (39 ppm) is substantially attributable to the inclusion for the first time of many cities in Africa, Asia, and South America, which tend to have higher LPD than urban areas elsewhere (Table 2). Our core result—a global population-weighted mean intraurban iF of 39 ppm—is approximately consistent with the estimated "archetypal" iF by Humbert et al. (49 ppm, breathing-rate-adjusted) for ground-level emissions.[8]

Model results for individual cities and countries agree favorably with those of previous studies after adjustment for differences in breathing rate. Overall, agreement is stronger for groups of cities (e.g., national averages of cities) than for individual urban areas. For example, our estimate for population-weighted mean intraurban iF for the 243 U.S. cities with populations ≥100 000 (21 ppm) is similar to the estimate of Marshall et al. (2005) for U.S. Census "urban areas" (17 ppm, breathing-rate-adjusted).[11] Likewise, our estimate for metropolitan Los Angeles (43 ppm) is consistent with an empirically derived iF estimate for the South Coast Air Basin (38 ppm, breathing-rate-adjusted).[12] Our results for Mexico City and Hong Kong—two cities with notoriously complex terrains—each differ from prior empirical estimates by ~50%, but in opposite directions. For Mexico City, our estimate (140 ppm) is ~60% larger than that of Stevens et al. (87 ppm, breathing-rate-adjusted).[13] In contrast, our estimate for Hong Kong (110 ppm) is ~40% lower than the value estimated by Luo et al.

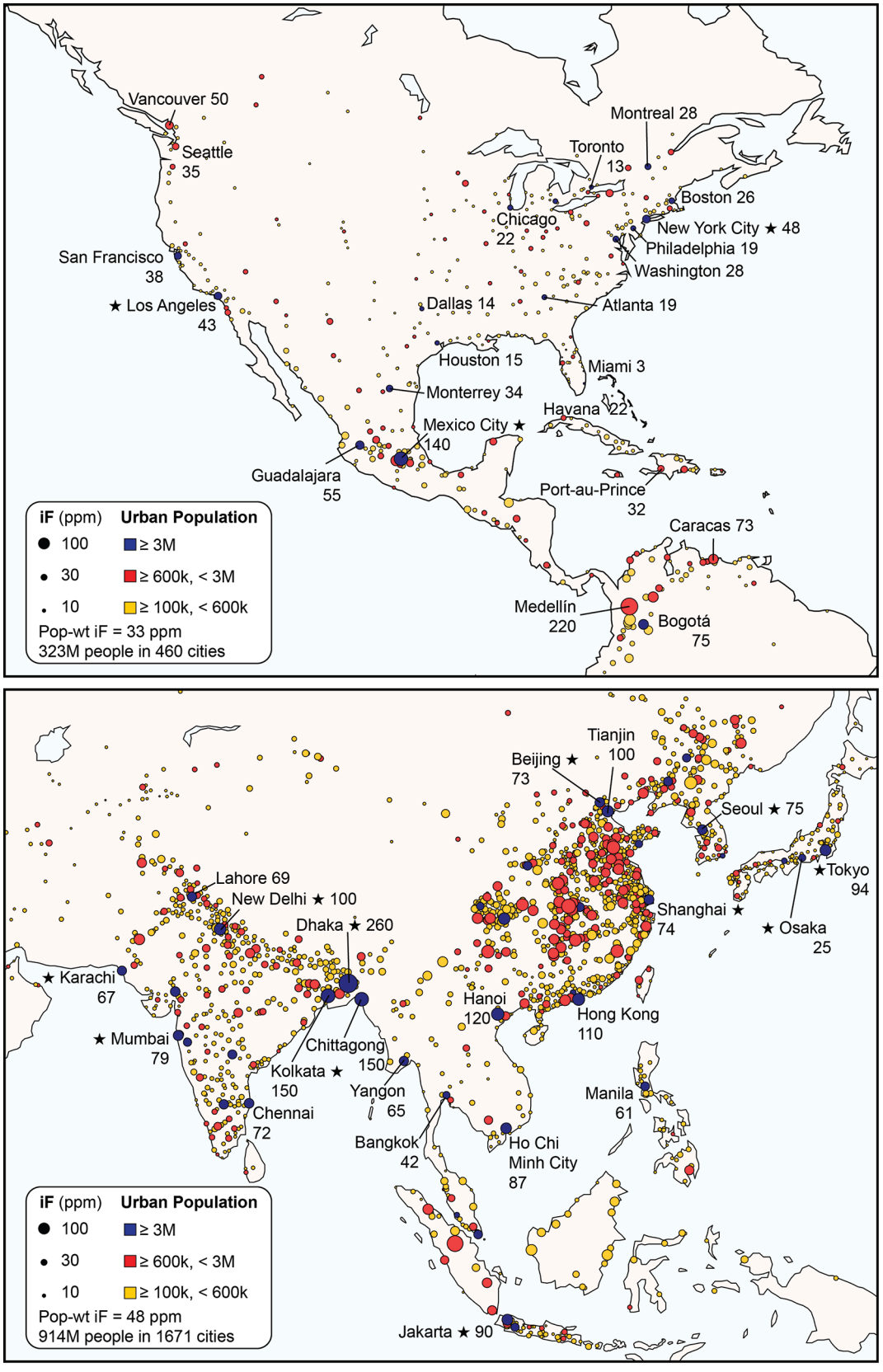

Figure 2. Map of intraurban intake fraction for cities in the Americas (upper panel) and Asia (lower panel). Values of iF are denoted by symbol area. City colors correspond with Figure 1 and indicate population size bins. Intake fractions for selected cities are labeled. Stars designate megacities (population >10 million, 11 on Asia map, 3 on Americas map). The same scale applies to both maps. The Supporting Information provides maps for other continents.

(190 ppm, breathing-rate-adjusted).[14] We obtain more closely comparable iF estimates for these two cities (to within ~±30%) after harmonizing demographic input parameters, which can vary substantially among studies of megacities.[57] Overall, the

dx.doi.org/10.1021/es204021h | *Environ. Sci. Technol.* 2012, 46, 3415–3423

results are consistent with an expectation of less than a factor of two uncertainty in iF values for individual cities estimated using the single-compartment Eulerian model.

While beyond the scope of the present study, further empirical validation of urban iF results is warranted. For example, emissions and concentration data for opportunistic tracer pollutants have already been used to develop semi-empirical iF estimates in several worldwide urban areas; for motor vehicles, example tracer species include CO, benzene, and diesel $PM_{2.5}$.[12−14,23,24] Recent improvements in global emissions data sets and satellite remote sensing techniques may permit more extensive use of empirical methods for assessing intake fractions in the future as a complement to the modeling approach employed here.

3.3. Sensitivity Analysis and Limitations. We tested the sensitivity of our results to many assumptions and modeling decisions that were necessary to assess iF at a global scale. On the basis of comparison with previous work (section 3.2), we estimate that the overall uncertainty for the aggregated (many-city) iF estimates is ∼30%.

Base-case analyses evaluate iF for nonreactive primary pollutants ($k = 0$). For nonconserved pollutants that follow first-order decay (half-lives 100 and 10 h), the mean iF is, respectively, only 0.8% and 7.2% lower than for conserved, nonreactive pollutants. The effect of decay was somewhat larger for large cities (11% for a 10 h half-life) owing to the longer residence time of air in cities with a greater length scale. Nevertheless, we found similar global patterns of iF with respect to region and city size for all three pollutant classes considered. Since the half-life for many health-relevant primary pollutants in urban air is larger than 10 h,[30] these findings imply that iF values for nonreactive pollutants may be reasonably applied to many toxic emissions to urban outdoor air. However, the iF values reported here may not be applicable to pollutants formed via secondary processes. For example, prior research indicates that intraurban iF may be 1−2 orders of magnitude lower for secondary $PM_{2.5}$ attributable to urban precursor emissions than for primary $PM_{2.5}$.[8−10]

In general, the results are relatively insensitive to most of the assumptions that we made in preprocessing meteorological parameters (section 2.3.1; Table SI.4, Supporting Information). However, the results for time-averaged iF are moderately sensitive to assumptions that relate to transient conditions of poor atmospheric mixing (e.g., during nights with low wind speeds). For example, the global mean iF is 35% lower in a sensitivity scenario under which the urban mixing height is constrained to be at least 100 m at all times. Since dispersion is generally weak at nights, alternative scenarios with higher emissions (E) or breathing rate (Q) at night result in higher iF values. The mean iF varies by 5−15% under a range of plausible assumptions about the diurnal pattern of E and Q (Table SI.5, Supporting Information). Refined model inputs for nighttime conditions may improve the accuracy of iF estimates in future studies.

An important modeling simplification relates to the aspect ratio, α, the ratio of an urban area's windward to crosswind dimensions (section 2.3.3). In the default modeling case, we assume square-plan layout ($\alpha = 1$), as α is not readily estimated for cities in this data set. In general, iF is expected to increase for situations where $\alpha > 1$ (less ventilation per unit land area), with the opposite true for $\alpha < 1$. The intake fraction for individual cities increased (decreased) by ∼30% for sensitivity cases in which $\alpha = 2$ ($\alpha = 0.5$). More detailed information on α may therefore improve the precision of iF estimates for individual cities.

The modeling approach employed here has limitations. The one-compartment model does not account for within-urban variation in exposure concentrations or for the effects of microenvironments. To the extent that exposures disproportionately occur in near-source regions (e.g., in vehicles on roads), iF may be systematically underestimated by the model. Conversely, the model may overestimate iF when outdoor-attributable indoor exposure concentrations are attenuated from ambient levels, as is the case for $PM_{2.5}$ encountered in buildings.[58] Considering limiting cases (see the Supporting Information), the effect of microenvironmental exposure modification is estimated to account for <30% absolute uncertainty, roughly consistent with estimates elsewhere.[12,38]

A further limitation is that the model only assesses intraurban iF, the fraction of a city's emissions that are inhaled by that city's own inhabitants. The results exclude additional intake that may occur in other urban or rural areas downwind of the source city and therefore may be considered a lower-bound estimate of total iF. Limited prior research suggests that intraurban iF for ground-level emissions may reasonably approximate the total iF in many circumstances.[20,59] Nevertheless, the difference between intraurban and total iF may be important in certain cases, such as for emissions in a small urban area that is located upwind and near large urban areas.

Since inhalation intake is an incomplete indicator of health risk, additional analyses are required to interpret iF results more explicitly in terms of health effects. In general, a metric of "intake-based toxicity" (IBT; sample units: mortality per mass intake) can be combined with iF to yield estimates of health effect per unit emission.[19,60] IBT may vary among populations. For example, similar reductions in intake may yield differential health benefits among populations with differing baseline exposure levels, susceptibilities, and underlying disease burdens.[61]

3.4. Implications for Policy. Given constrained resources for environmental protection, air quality policies may seek to maximize the environmental health benefit achieved per unit cost expended. Intake fraction lends insight into one dimension of this calculus: the population intake benefit associated with a given quantity of emissions reduction. In concert with other information routinely used in air quality management and health risk assessment (e.g., source strengths, cost-of-control curves, pollutant toxicity data), it may be advantageous to prioritize emissions reductions for sources with high iF.[10,62−64] The global average iF for urban vehicle emissions (39 ppm) is substantially greater than previous estimates of iF for central electric power stations located in California, U.S. (∼1 ppm),[20] or China (∼10 ppm),[21] reinforcing the relative importance of vehicle emissions control. Comparing among regions, our results suggest that mitigating or avoiding increases in urban vehicle emissions in countries with high iF (e.g., India, China, and Indonesia) may yield relatively high exposure-reduction benefits per unit of emissions reduction. Moreover, as vehicle fleets in these countries tend to be high emitting and rapidly growing, the marginal costs of emissions abatement may be favorable. The exposure benefits of emissions control in megacities also appear particularly strong. Intake fraction results by season and time of day suggest that emissions control measures for ground-level sources with high emissions at night (e.g., trucking)[65] or during the winter (e.g., solid-fuel combustion for heat)[24,56] may yield relatively high exposure benefits per unit mitigation.

■ ASSOCIATED CONTENT

Supporting Information

Additional description of the methodology and results, including figures and tables of urban- and national-level iF data. This material is available free of charge via the Internet at http://pubs.acs.org/

■ AUTHOR INFORMATION

Corresponding Author

*E-mail: julian@umn.edu; phone: (612) 625-2397; fax: (612) 626-7750.

Notes

The funding agencies neither reject nor endorse the conclusions and views expressed herein.

The authors declare no competing financial interest.

■ ACKNOWLEDGMENTS

We thank S. Angel, M. Bechle, K. Smith, and C. Tessum for assistance with the model input data and helpful feedback. This research was funded in part by the U.S. EPA STAR graduate fellowship program, the Energy Biosciences Institute at the University of California, Berkeley, and the International Council on Clean Transportation.

■ REFERENCES

(1) Pope, C. A.; Dockery, D. W. Health effects of fine particulate air pollution: Lines that connect. *J. Air Waste Manage. Assoc.* **2006**, *56*, 709−742.

(2) Pope, C. A.; Ezzati, M.; Dockery, D. W. Fine-particulate air pollution and life expectancy in the United States. *N. Engl. J. Med.* **2009**, *360*, 376−386.

(3) Kampa, M.; Castanas, E. Human health effects of air pollution. *Environ. Pollut.* **2008**, *151*, 362−367.

(4) *Global Health Risks: Mortality and Burden of Disease Attributable to Selected Major Risks*; World Health Organization: Geneva, Switzerland, 2009; http://www.who.int/healthinfo/global_burden_disease/GlobalHealthRisks_report_full.pdf. Accessed: Feb 24, 2012.

(5) Bennett, D. H.; McKone, T. E.; Evans, J. S.; Nazaroff, W. W.; Margni, M. D.; Jolliet, O.; Smith, K. R. Defining intake fraction. *Environ. Sci. Technol.* **2002**, *36*, 206A−211A.

(6) Lai, A. C. K.; Thatcher, T. L.; Nazaroff, W. W. Inhalation transfer factors for air pollution health risk assessment. *J. Air Waste Manage. Assoc.* **2000**, *50*, 1688−1699.

(7) Rosenbaum, R. K.; Margni, M.; Jolliet, O. A flexible matrix algebra framework for the multimedia multipathway modeling of emission to impacts. *Environ. Int.* **2007**, *33*, 624−634.

(8) Humbert, S.; Marshall, J. D.; Shaked, S.; Spadaro, J. V.; Nishioka, Y.; Preiss, P.; McKone, T. E.; Horvath, A.; Jolliet, O. Intake fraction for particulate matter: Recommendations for life cycle impact assessment. *Environ. Sci. Technol.* **2011**, *45*, 4808−4816.

(9) Greco, S. L.; Wilson, A. M.; Spengler, J. D.; Levy, J. I. Spatial patterns of mobile source particulate matter emissions-to-exposure relationships across the United States. *Atmos. Environ.* **2007**, *41*, 1011−1025.

(10) Evans, J. S.; Wolff, S. K.; Phonboon, K.; Levy, J. I.; Smith, K. R. Exposure efficiency: An idea whose time has come? *Chemosphere* **2002**, *49*, 1075−1091.

(11) Marshall, J. D.; Teoh, S. K.; Nazaroff, W. W. Intake fraction of nonreactive vehicle emissions in US urban areas. *Atmos. Environ.* **2005**, *39*, 1363−1371.

(12) Marshall, J. D.; Riley, W. J.; McKone, T. E.; Nazaroff, W. W. Intake fraction of primary pollutants: Motor vehicle emissions in the South Coast Air Basin. *Atmos. Environ.* **2003**, *37*, 3455−3468.

(13) Stevens, G.; de Foy, B.; West, J. J.; Levy, J. I. Developing intake fraction estimates with limited data: Comparison of methods in Mexico City. *Atmos. Environ.* **2007**, *41*, 3672−3683.

(14) Luo, Z.; Li, Y.; Nazaroff, W. W. Intake fraction of nonreactive motor vehicle exhaust in Hong Kong. *Atmos. Environ.* **2010**, *44*, 1913−1918.

(15) Baidya, S.; Borken-Kleefeld, J. Atmospheric emissions from road transportation in India. *Energy Policy* **2009**, *37*, 3812−3822.

(16) Pucher, J.; Korattyswaropam, N.; Mittal, N.; Ittyerah, N. Urban transport crisis in India. *Transp. Policy* **2005**, *12*, 185−198.

(17) Chang, D.; Song, Y.; Liu, B. Visibility trends in six megacities in China 1973−2007. *Atmos. Res.* **2009**, *94*, 161−167.

(18) He, K.; Huo, H.; Zhang, Q.; He, D.; An, F.; Wang, M.; Walsh, M. P. Oil consumption and CO_2 emissions in China's road transport: Current status, future trends, and policy implications. *Energy Policy* **2005**, *33*, 1499−1507.

(19) Ji, S.; Cherry, C. R.; Bechle, M. J.; Wu, Y.; Marshall, J. D. Electric vehicles in China: Emissions and health impacts. *Environ. Sci. Technol.* **2012**, *46*, 2018−2024.

(20) Heath, G. A.; Granvold, P. W.; Hoats, A. S.; Nazaroff, W. W. Intake fraction assessment of the air pollutant exposure implications of a shift toward distributed electricity generation. *Atmos. Environ.* **2006**, *40*, 7164−7177.

(21) Zhou, Y.; Levy, J. I.; Evans, J. S.; Hammitt, J. K. The influence of geographic location on population exposure to emissions from power plants throughout China. *Environ. Int.* **2006**, *32*, 365−373.

(22) Tainio, M.; Sofiev, M.; Hujo, M.; Tuomisto, J. T.; Loh, M.; Jantunen, M. J.; Karppinen, A.; Kangas, L.; Karvosenoja, N.; Kupiainen, K.; Porvari, P.; Kukkonen, J. Evaluation of the European population intake fractions for European and Finnish anthropogenic primary fine particulate matter emissions. *Atmos. Environ.* **2009**, *43*, 3052−3059.

(23) Loh, M. M.; Soares, J.; Karppinen, A.; Kukkonen, J.; Kangas, L.; Riikonen, K.; Kousa, A.; Asikainen, A.; Jantunen, M. J. Intake fraction distributions for benzene from vehicles in the Helsinki metropolitan area. *Atmos. Environ.* **2009**, *43*, 301−310.

(24) Ries, F. J.; Marshall, J. D.; Brauer, M. Intake fraction of urban wood smoke. *Environ. Sci. Technol.* **2009**, *43*, 4701−4706.

(25) Marshall, J. D.; Behrentz, E. Vehicle self-pollution intake fraction: Children's exposure to school bus emissions. *Environ. Sci. Technol.* **2005**, *39*, 2559−2563.

(26) Stevens, G.; Wilson, A.; Hammitt, J. K. A benefit-cost analysis of retrofitting diesel vehicles with particulate filters in the Mexico City metropolitan area. *Risk Anal.* **2005**, *25*, 883−899.

(27) Bennett, D. H.; Margni, M. D.; McKone, T. E.; Jolliet, O. Intake fraction for multimedia pollutants: A tool for life cycle analysis and comparative risk assessment. *Risk Anal.* **2002**, *22*, 905−918.

(28) Cahill, T. M.; Mackay, D. Complexity in multimedia mass balance models: When are simple models adequate and when are more complex models necessary? *Environ. Toxicol. Chem.* **2003**, *22*, 1404−1412.

(29) Seinfeld, J. H.; Pandis, S. N. *Atmospheric Chemistry and Physics: From Air Pollution to Climate Change*, 2nd ed.; Wiley-Interscience: Hoboken, NJ, 2006.

(30) Atkinson, R. Atmospheric chemistry of VOCs and NO_x. *Atmos. Environ.* **2000**, *34*, 2063−2101.

(31) Rienecker, M. M.; Suarez, M. J.; Gelaro, R.; Todling, R.; Bacmeister, J.; Liu, E.; Bosilovich, M. G.; Schubert, S. D.; Takacs, L.; Kim, G.-K.; Bloom, S.; Chen, J.; Collins, D.; Conaty, A.; da Silva, A.; Gu, W.; Joiner, J.; Koster, R. D.; Lucchesi, R.; Molod, A.; Owens, T.; Pawson, S.; Pegion, P.; Redder, C. R.; Reichle, R.; Robertson, F. R.; Ruddick, A. G.; Sienkiewicz, M.; Woollen, J. MERRA: NASA's Modern-Era Retrospective Analysis for Research and Applications. *J. Clim.* **2011**, *24*, 3624−3648.

(32) Hanna, S. R.; Briggs, G. A.; Hosker, R. P., Jr. *Handbook on Atmospheric Diffusion*; DOE/TIC-112233; Office of Energy and Research, U.S. Department of Energy: Washington, DC, 1982; http://www.orau.org/ptp/PTP Library/library/Subject/Meteorology/handbook on atmospheric diffusion.pdf. Accessed: Feb 24, 2012.

(33) Irwin, J. S. A theoretical variation of the wind profile power-law exponent as a function of surface roughness and stability. *Atmos. Environ.* **1979**, *13*, 191−194.

(34) Stephenson, R.; Mohan, R. M.; Duffin, J.; Jarsky, T. M. Circadian rhythms in the chemoreflex control of breathing. *Am. J. Physiol.: Regul., Integr. Comp. Physiol.* **2000**, *278*, R282−R286.
(35) *Exposure Factors Handbook: 2009 Update (External Review Draft)*; EPA/600/R-09/052A; U.S. Environmental Protection Agency: Washington, DC, 2009; http://cfpub.epa.gov/ncea/cfm/recordisplay.cfm?deid=209866. Accessed: Feb 24, 2012.
(36) *Metabolically Derived Human Ventilation Rates: A Revised Approach Based upon Oxygen Consumption Rates*; EPA/600/R-06/129F; U.S. Environmental Protection Agency, National Center for Environmental Assessment: Washington, DC, 2009; http://cfpub.epa.gov/ncea/cfm/recordisplay.cfm?deid=202543. Accessed: Feb 24, 2012.
(37) Klepeis, N. E.; Nelson, W. C.; Ott, W. R.; Robinson, J. P.; Tsang, A. M.; Switzer, P.; Behar, J. V.; Hern, S. C.; Engelmann, W. H. The National Human Activity Pattern Survey (NHAPS): A resource for assessing exposure to environmental pollutants. *J. Exposure Anal. Environ. Epidemiol.* **2001**, *11*, 231−252.
(38) Marshall, J. D.; Granvold, P. W.; Hoats, A. S.; McKone, T. E.; Deakin, E.; Nazaroff, W. W. Inhalation intake of ambient air pollution in California's South Coast Air Basin. *Atmos. Environ.* **2006**, *40*, 4381−4392.
(39) Angel, S.; Parent, J.; Civco, D.; Blei, A.; Potere, D. *A Planet of Cities: Urban Land Cover Estimates and Projections for All Countries, 2000−2050*; WP10SA3; Lincoln Institute of Land Policy: Cambridge, MA, 2010; http://www.lincolninst.edu/pubs/1861_A-Planet-of-Cities. Accessed: Feb 24, 2012.
(40) Angel, S.; Parent, J.; Civco, D. L.; Blei, A.; Potere, D. The dimensions of global urban expansion: Estimates and projections for all countries, 2000−2050. *Prog. Plann.* **2011**, *75*, 53−107.
(41) Schneider, A.; Friedl, M. A.; Potere, D. A new map of global urban extent from MODIS satellite data. *Environ. Res. Lett.* **2009**, *4*, 044003.
(42) Potere, D.; Schneider, A.; Angel, S.; Civco, D. L. Mapping urban areas on a global scale: Which of the eight maps now available is more accurate? *Int. J. Remote Sens.* **2009**, *30*, 6531−6558.
(43) Huo, H.; Zhang, Q.; He, K.; Wang, Q.; Yao, Z.; Streets, D. G. High-resolution vehicular emission inventory using a link-based method: A case study of light-duty vehicles in Beijing. *Environ. Sci. Technol.* **2009**, *43*, 2394−2399.
(44) Guttikunda, S. K. Diurnal profiles for Delhi emissions inventory, personal communication, June 8, 2011.
(45) *The National Emissions Inventory*; U.S. Environmental Protection Agency: Washington, DC, 2011; http://www.epa.gov/ttn/chief/net/2008inventory.html. Accessed: Feb 24, 2012.
(46) Marshall, J. D. Urban land area and population growth: A new scaling relationship for metropolitan expansion. *Urban Stud.* **2007**, *44*, 1889−1904.
(47) Mage, D.; Ozolins, G.; Peterson, P.; Webster, A.; Orthofer, R.; Vandeweerd, V.; Gwynne, M. Urban air pollution in megacities of the world. *Atmos. Environ.* **1996**, *30*, 681−686.
(48) Guttikunda, S. K.; Tang, Y.; Carmichael, G. R.; Kurata, G.; Pan, L.; Streets, D. G.; Woo, J.-H.; Thongboonchoo, N.; Fried, A. Impacts of Asian megacity emissions on regional air quality during spring 2001. *J. Geophys. Res.* **2005**, *110*, D20301.
(49) Gurjar, B. R.; Butler, T. M.; Lawrence, M. G.; Lelieveld, J. Evaluation of emissions and air quality in megacities. *Atmos. Environ.* **2008**, *42*, 1593−1606.
(50) Butler, T. M.; Lawrence, M. G.; Gurjar, B. R.; van Aardenne, J.; Schultz, M.; Lelieveld, J. The representation of emissions from megacities in global emission inventories. *Atmos. Environ.* **2008**, *42*, 703−719.
(51) Gurjar, B. R.; Lelieveld, J. New directions: Megacities and global change. *Atmos. Environ.* **2005**, *39*, 391−393.
(52) Parrish, D. D.; Zhu, T. Clean air for megacities. *Science* **2009**, *326*, 674−675.
(53) Molina, M. J.; Molina, L. T. Megacities and atmospheric pollution. *J. Air Waste Manage. Assoc.* **2004**, *54*, 644−680.
(54) Wang, H.; Fu, L.; Zhou, Y.; Du, X.; Ge, W. Trends in vehicular emissions in China's mega cities from 1995 to 2005. *Environ. Pollut.* **2010**, *158*, 394−400.
(55) Chan, C. K.; Yao, X. Air pollution in mega cities in China. *Atmos. Environ.* **2008**, *42*, 1−42.
(56) Taimisto, P.; Tainio, M.; Karvosenoja, N.; Kupiainen, K.; Porvari, P.; Karppinen, A.; Kangas, L.; Kukkonen, J.; Tuomisto, J. Evaluation of intake fractions for different subpopulations due to primary fine particulate matter ($PM_{2.5}$) emitted from domestic wood combustion and traffic in Finland. *Air Qual. Atmos. Health* **2011**, *4*, 199−209.
(57) Forstall, R. L.; Greene, R. P.; Pick, J. B. Which are the largest? Why lists of major urban areas vary so greatly. *Tijdschr. Econ. Soc. Geogr.* **2009**, *100*, 277−297.
(58) Riley, W. J.; McKone, T. E.; Lai, A. C. K.; Nazaroff, W. W. Indoor particulate matter of outdoor origin: Importance of size-dependent removal mechanisms. *Environ. Sci. Technol.* **2002**, *36*, 200−207.
(59) Greco, S. L.; Wilson, A. M.; Hanna, S. R.; Levy, J. I. Factors influencing mobile source particulate matter emissions-to-exposure relationships in the Boston urban area. *Environ. Sci. Technol.* **2007**, *41*, 7675−7682.
(60) Marshall, J. D.; Nazaroff, W. W. Risk assessment of diesel-fired back-up electric generators operating in California, 2002; Appendix 4-2. http://z.umn.edu/dieselBUG. Accessed: Feb 24, 2012.
(61) Levy, J. I.; Greco, S. L.; Melly, S. J.; Mukhi, N. Evaluating efficiency-equality tradeoffs for mobile source control strategies in an urban area. *Risk Anal.* **2009**, *29*, 34−47.
(62) Roumasset, J. A.; Smith, K. R. Exposure trading: An approach to more efficient air pollution control. *J. Environ. Econ. Manage.* **1990**, *18*, 276−291.
(63) Smith, K. R. Fuel combustion, air pollution exposure, and health: The situation in developing countries. *Annu. Rev. Energy Environ.* **1993**, *18*, 529−566.
(64) Nazaroff, W. W. New directions: It's time to put the human receptor into air pollution control policy. *Atmos. Environ.* **2008**, *42*, 6565−6566.
(65) Sathaye, N.; Harley, R.; Madanat, S. Unintended environmental impacts of nighttime freight logistics activities. *Transp. Res. A* **2010**, *44*, 642−659.

Supplementary Information

Global intraurban intake fractions for primary air pollutants from vehicles and other distributed sources

Joshua S. Apte [a], Emilie Bombrun [b], Julian D. Marshall [b,*], and William W Nazaroff [c]

[a] Energy and Resources Group, University of California, Berkeley, CA, 94720-3050 USA

[b] Department of Civil Engineering, University of Minnesota, Minneapolis, MN 55455-0233 USA

[c] Department of Civil and Environmental Engineering, University of California, Berkeley, CA, 94720-1710 USA

Contents

Pages: 21
Figures: 10
Tables: 9

[*] Corresponding author. E-mail: julian@umn.edu. Phone: 612-625-2397. Fax: 612-626-7750. Address: 500 Pillsbury Drive SE, University of Minnesota, Minneapolis MN 55455-0233 USA

SI.1 Methods

SI.1.1 Vertical wind profile

MERRA data provide wind speed at a standard 10-meter height. We use the following truncated power-law relationship to evaluate wind speed at a specific time ($u(z,t)$; units: m s^{-1}) as a function of height (z, units: m).[1-3]

$$u\left(z,t\right) = u_{\text{ref}}(t) \times \left(\frac{z}{H_{\text{ref}}}\right)^{p} \quad \text{for } z \le H_{\text{max}} \qquad \text{SI.1a}$$

$$u\left(z,t\right) = \text{constant} = u_{\text{ref}}(t) \times \left(\frac{H_{\text{max}}}{H_{\text{ref}}}\right)^{p} \quad \text{for } z > H_{\text{max}} \qquad \text{SI.1b}$$

Here, $u_{\text{ref}}(t)$ is the wind speed (m s^{-1}) at the reference height at a specific time, H_{ref} is the reference height (10 m), H_{max} is the cutoff height (m) above which wind speed is assumed constant, and p is an empirical constant (dimensionless) that can vary with surface roughness and atmospheric stability. We employed 200 m as the cutoff height[1] and p = 0.32, which is an appropriate value for neutrally stable conditions in urban areas.[3-5] In sensitivity analysis, we consider alternate values for the cutoff height (H_{max} = 100 m, ∞) and the wind profile exponent (p = 0.25, 0.37, which covers a range of stability conditions). To obtain the time-dependent mixing-depth averaged wind speed $u(t)$, we evaluate the following integral:

$$u(t) = \frac{1}{H(t)} \int_{0}^{H(t)} u\left(z,t\right) dz \qquad \text{SI.2}$$

Substituting equations SI.1a-b into equation SI.2, the following analytic solutions are found:

$$u(t) = \frac{u_{\text{ref}}(t)}{p+1} \left(\frac{H(t)}{H_{\text{ref}}}\right)^{p} \qquad \text{for } z \le H_{\text{max}} \qquad \text{SI.3a}$$

$$u(t) = \frac{H_{max}\left[\frac{u_{ref}(t)}{p+1}\times\left(\frac{H_{max}}{H_{ref}}\right)^{p}\right] + \left(H(t)-H_{max}\right)\left[u_{ref}(t)\times\left(\frac{H_{max}}{H_{ref}}\right)^{p}\right]}{H(t)} \quad \text{for } z > H_{max} \quad \text{SI.3b}$$

SI.1.2 Diurnal breathing rate profile

The diurnal profile of population mean breathing rate (units: $m^3\ d^{-1}\ person^{-1}$) is attributable to temporal profile of activity intensity within a population. For example, population mean breathing rate is lower at night, when much of the population is sleeping. The US Environmental Protection Agency (US EPA) provides activity-specific estimates of mean instantaneous breathing rate for discrete age groups.[6] Activities are clustered into five intensity levels: "sleep/nap," "sedentary," "light," "moderate," and "heavy." We used US Census Bureau population age structure data for 2009 (http://www.census.gov/popest/national/asrh/NC-EST2009-sa.html) to eliminate the age-dependence of the US EPA breathing rate dataset, resulting in population mean breathing rates for each of the five activity levels. Mean breathing rates were only slightly sensitive to the age distribution employed. For example, compared to the default age distribution (US, mean age: 37 y), mean activity-specific breathing rates for the Japanese and Indian population-age distributions (mean ages: 44, 28 y) differed by ±1-4%. Table SI.1 provides estimates of mean breathing rate and hours spent at each activity level for the US population.

Table SI.1. Activity-specific breathing rates for the US population [a]

Activity Mode	Breathing rate (m^3 person^{-1} d^{-1})	Time spent (h d^{-1})
Sleep / Nap	6.9	8.8
Sedentary	6.8	4.5
Light	17	6.3
Moderate	37	4.1
Heavy	69	0.3

[a] Adapted from US EPA data[6]

We used data from the US National Human Activity Pattern Survey (NHAPS)[7] to convert activity-specific inhalation rates into an estimate of the diurnal profile of population breathing rate. For each hour of the day, NHAPS reports the distribution of the US population by microenvironment. We categorized microenvironments into four groups: indoor-residence, vehicles, other indoor, and outdoors (Figure SI.1). For each microenvironment and hour of the day, we made best-judgment estimates of the fraction of population-time spent at each activity level. We used the data in Table SI.1 as a constraint on the total person-time that could be spent at each activity level over the course of a day. The results of this apportionment are summarized in Table SI.2 and Figure SI.2. Finally, activity-specific breathing rates in Table SI.1 were applied to the diurnal activity profile (Figure SI.2), resulting in the diurnal breathing rate profile depicted in Figure SI.3. The time-weighted average breathing rate for this constructed diurnal profile is 15.4 m^3 $person^{-1}$ d^{-1}. To match the long-term population mean breathing rate recommended by the US EPA Exposure Factors Handbook (14.5 m^3 $person^{-1}$ d^{-1}),[8] we applied a constant scaling factor of 0.94 to the population breathing rate at each hour of the day.

To test the sensitivity of results to the breathing rate profile, we considered four alternate temporal patterns of population breathing rate (Figure SI.4): (a) time-invariant ("flat"); (b) a sinusoidal daily cycle ("sine wave") with amplitude set at ± 25% of the mean, minimum (maximum) at 0600 h (1800 h);[9] and two profiles developed by Marshall et al. for the population of the South Coast Air Basin (in the Los Angeles, USA region) based (c) on author assumptions ("SoCAB-1")[10] and (d) a local time-activity survey ("SoCAB-2").[11] Compared with the base case, all sensitivity cases except SoCAB-1 assume relatively more population inhalation during night hours (2100 h – 0300h) and less inhalation during daytime hours (0900 h – 1500 h, Figure SI.4).

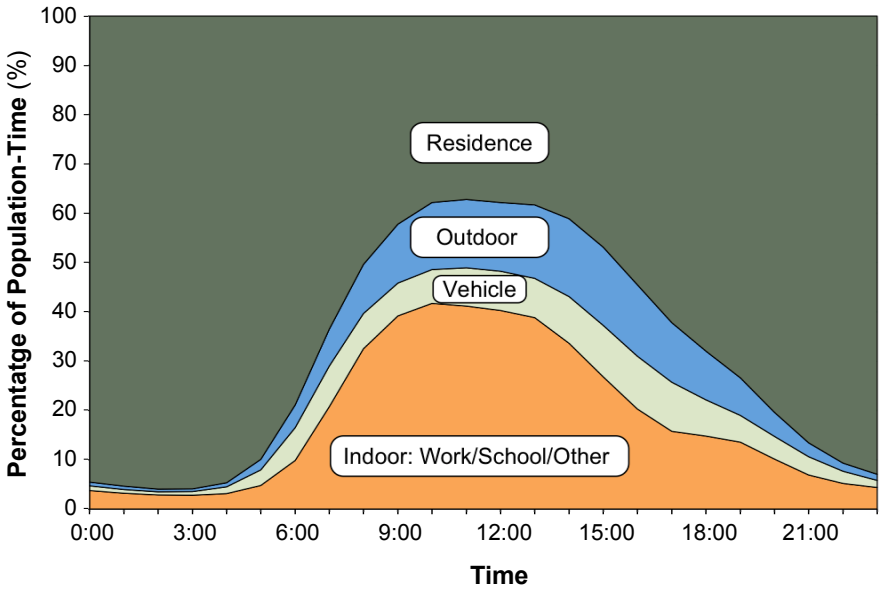

Figure SI.1. Fraction of total person time in NHAPS for each of four microenvironment groupings.

Table SI.2. Apportionment of average person time (h d^{-1}) by microenvironment and breathing rate for US population in NHAPS

	Sleep	Sedentary	Light	Moderate	High	Total
Residence	8.7	2.5	3.4	1.8	0.15	**16**
Other Indoor	0.13	1.2	2.0	1.0	0.04	**4.4**
In-Vehicle	-	0.53	0.53	0.26	-	**1.3**
Outdoor	-	0.22	0.45	1.0	0.11	**1.8**
Total	**8.8**	**4.5**	**6.3**	**4.1**	**0.30**	**24**

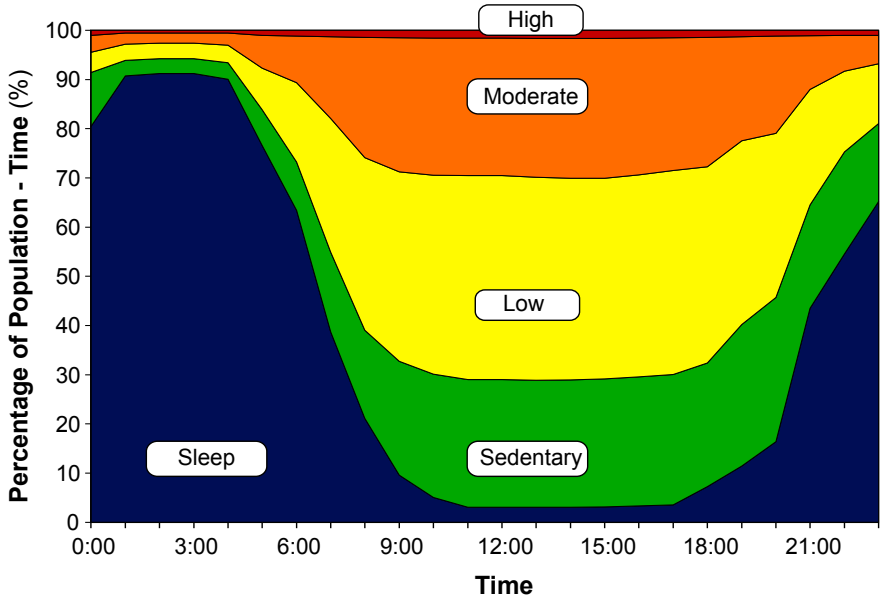

Figure SI.2. Estimated fraction of US population-time in each of five breathing rate modes by hour of day.

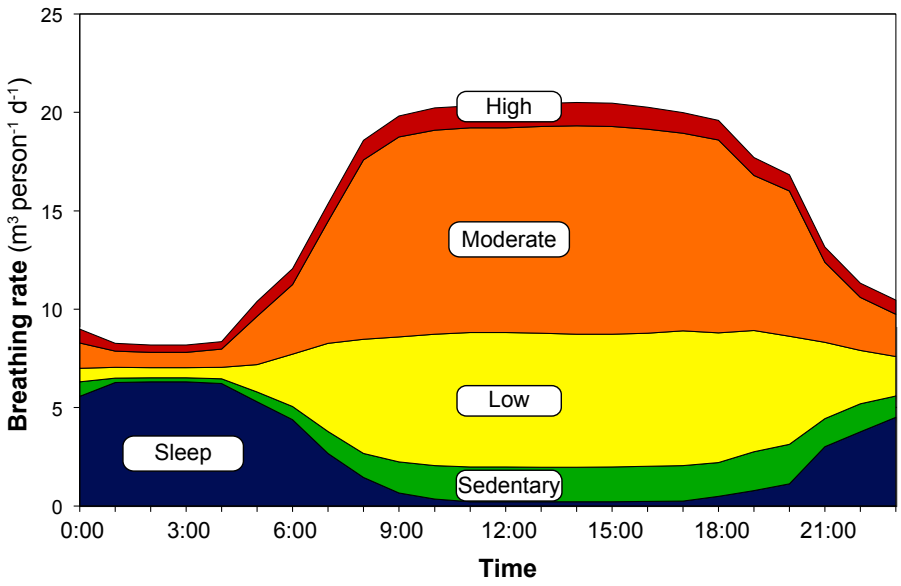

Figure SI.3. Diurnal breathing rate profile for the US population estimated using US EPA and NHAPS data.

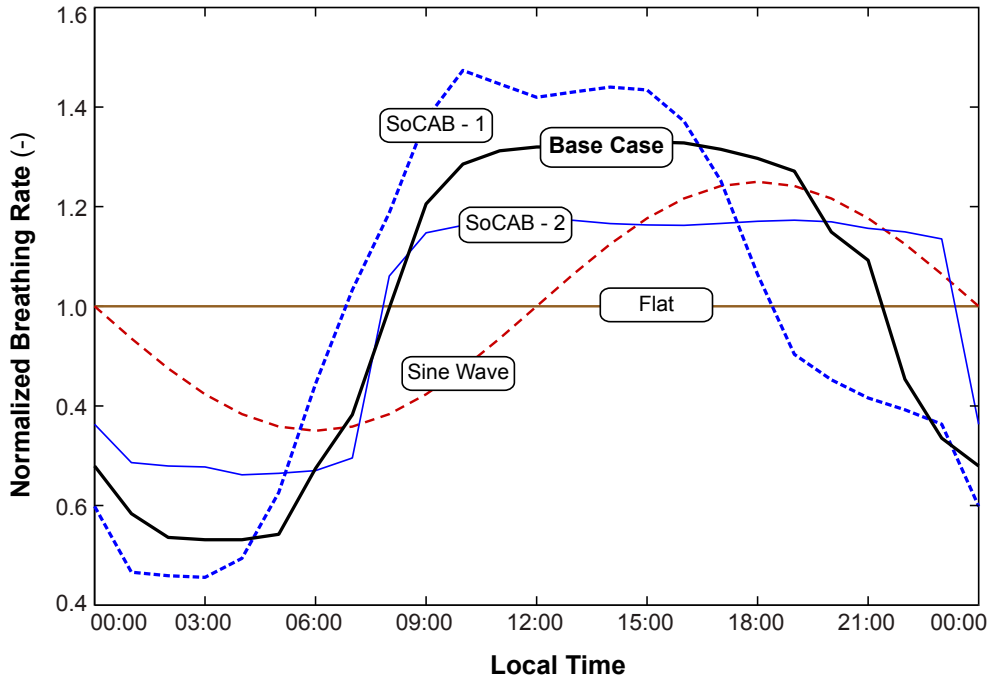

Figure SI.4. Comparison of base case diurnal breathing rate profile with three alternate profiles used for sensitivity analysis. All profiles are normalized to time-averaged breathing rate (14.5 m^3 $person^{-1}$ d^{-1}).

SI.1.3 Diurnal emissions profile

Diurnal profiles of vehicle emissions depend on temporal patterns in the activity and composition of a vehicle fleet. Moreover, emissions profiles vary among cities and pollutants. Detailed data on the diurnal timing of vehicle emissions are not available for a large sample of global cities. However, we expect some commonalities among the emissions profiles. First, vehicle activity (vehicle-km h^{-1}) is typically greatest during daytime hours. Second, especially in large cities, the relative abundance of heavy-duty vehicles (HDV) is often higher at night, owing to traffic conditions, logistics considerations or local regulations.[12-14] For many pollutants (e.g., $PM_{2.5}$), HDV have higher emissions factors (g emission per vehicle-km) than do light-duty vehicles (LDV). Accordingly, the diurnal profile of emissions from all vehicle classes is typically less variable than the diurnal profile of vehicle activity.

The base-case emissions profile is defined as the average of the diurnal profiles (dimensionless, relative emissions per hour) for Mexico City, Mexico ($PM_{2.5}$, all mobile sources),[2] New Delhi, India (CO, all mobile sources),[14] and Beijing, China (CO, LDV).[15] Sensitivity of results to the choice of diurnal profile was tested using the following alternative cases (Fig SI.5): (a) time-invariant emissions ("flat"), (b) individual diurnal profiles from the above cities, and (c) diurnal vehicle activity data (LDV+HDV vehicle km h^{-1}) from the US EPA National Emissions Inventory ("USA NEI").[16] Among all profiles considered, the "flat" and New Delhi emissions profiles have the highest relative emissions during nighttime and lowest relative emissions during daytime, while the reverse is true for the USA NEI activity dataset.

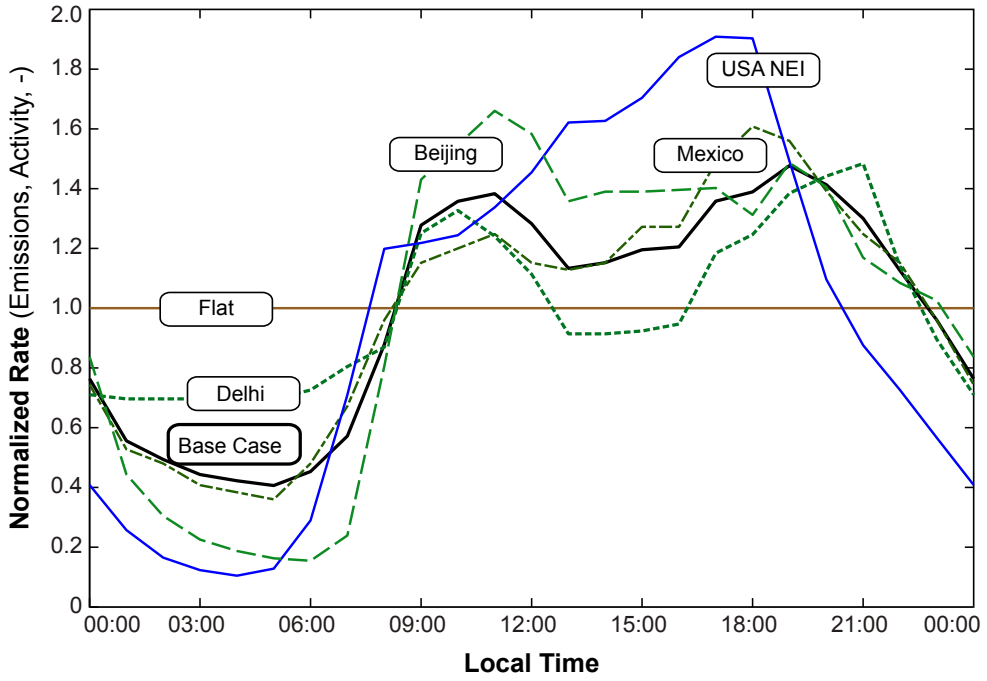

Figure SI.5. Comparison of base case diurnal emissions profile with alternate profiles used for sensitivity analysis. Profiles represent the normalized hourly emissions rate (dimensionless); for a given diurnal profile, *iF* is independent of the total quantity released. The base case diurnal profile represents the simple average of normalized diurnal emissions profiles for Beijing, Delhi, and Mexico City. USA NEI profile reflects hourly vehicle fleet activity (vehicle km^{-1}).

SI.2 Results and Discussion

SI.2.1 Supplementary data: core analyses

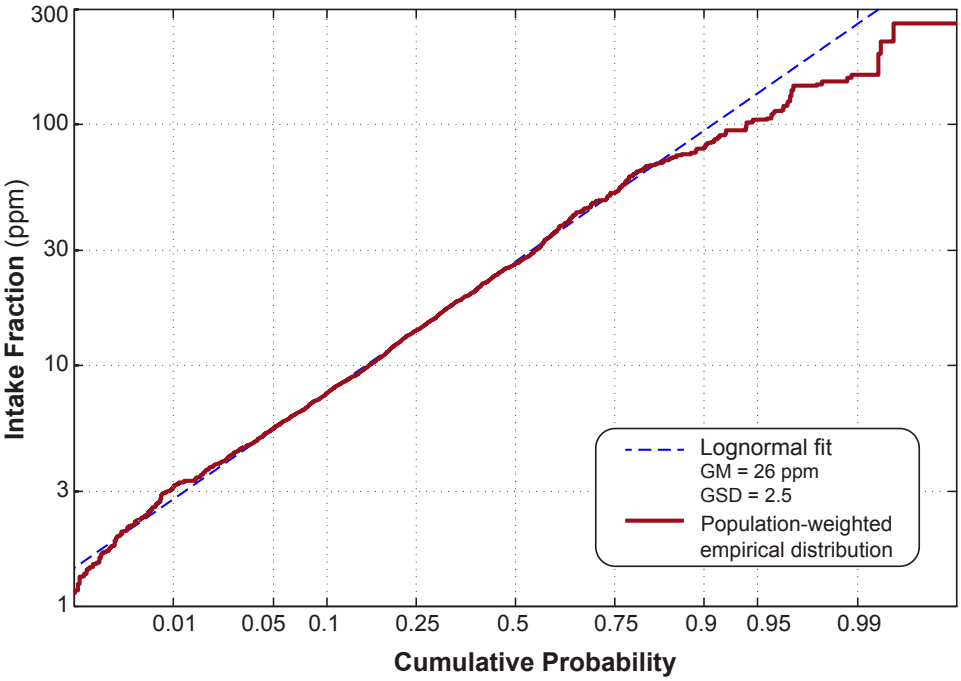

Figure SI.6. Log-probability plot for population-weighted global distribution of *iF*. The empirical cumulative distribution of *iF* is reasonably approximated by a lognormal fit ($r^2 = 0.92$), with excellent fit for the lower 75% of the population-weighted distribution of *iF*.

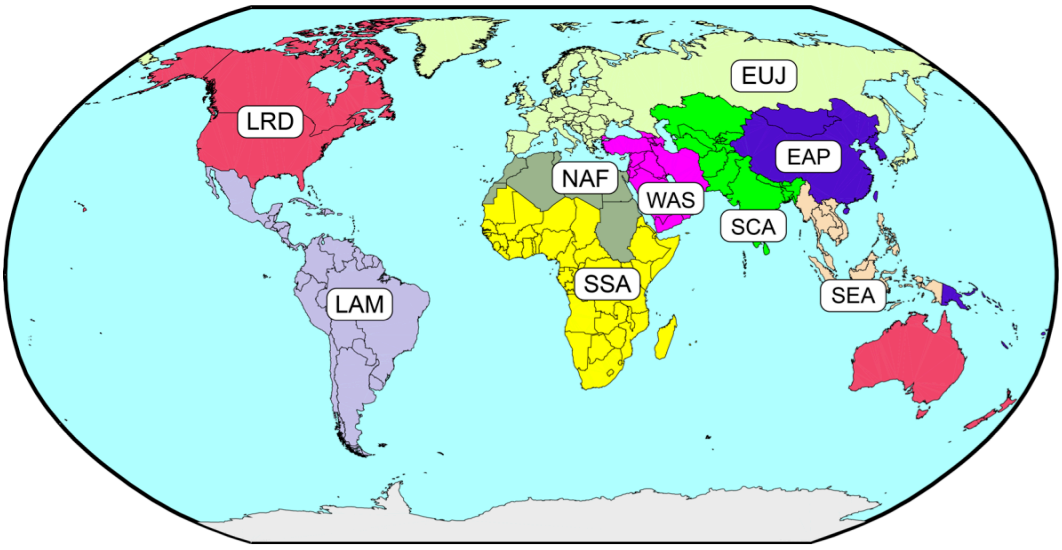

Figure SI.7. Map of nine world regions used for analysis, after Angel et al.[17, 18] See Table SI.3 for definition of region codes.

Table SI.3. Population-weighted mean intake fraction (*iF*) by region and city size [a]

	Region	*iF* (ppm)			Population (million)			Number of Cities		
		S	M	L	S	M	L	S	M	L
SCA	South and Central Asia	14.9	35.5	106	93.5	88.7	105	450	76	13
SEA	Southeast Asia	19.8	45.8	67.1	33.2	22.3	51.8	165	22	9
EAP	East Asia and Pacific	21.8	49.3	70.4	165	194	99.3	716	161	14
SSA	sub-Saharan Africa	17.9	38.2	98.3	43.4	63.5	25.1	202	52	4
LAM	Latin America	12.7	32.2	68.8	68.8	93.3	96.8	318	73	12
NAF	North Africa	10.0	26.5	56.8	20.4	11.5	21.2	103	8	4
EUJ	Europe and Japan	10.1	21.8	55.4	146	111	143	681	97	18
WAS	Western Asia	12.3	26.6	41.0	29.2	35.5	24.8	125	27	5
LRD	land-rich developed	6.6	14.9	30.1	49.9	67.1	109	222	53	16

[a] Cities sorted by population size range: (S) – small, 100,000 ≤ population < 600,000; (M) – medium, 600,000 ≤ population < 3,000,000; (L) – large, population ≥ 3,000,000.

SI.2.2 Sensitivity analyses

SI.2.2.1 – Tables of sensitivity scenario results

Table SI.4. Sensitivity of model results to meteorological inputs. [a]

Model Parameter	Mean [b]	P_{25} [c]	P_{75} [c]
Wind profile cap (default: H_{max} = 200 m)			
H_{max} = 100 m	+ 1.8%	+ 1.0%	+ 3.0%
H_{max}= 150 m	+ 0.6%	+ 0.4%	+ 1.0%
H_{max} = 300 m	- 0.6%	- 1.1%	- 0.4%
H_{max} = ∞	- 1.6%	- 2.4%	- 0.9%
Wind profile exponent (default: p = 0.32)			
p = 0.25	+ 7.9%	- 6.5%	+ 9.2%
p = 0.37	- 5.4%	- 6.2%	- 4.5%
Year of meteorological data	(default: 2007 - 2009)		
2007	- 0.4%	- 5.9%	+ 5.6%
2008	+ 0.1%	- 5.1%	+ 4.7%
2009	+ 0.3%	- 5.3%	+ 6.4%

[a] Sensitivity is defined as $100 \times (iF_{sens\_case} - iF_{base\_case}) / iF_{base\_case,}$ where iF_{sens_case} and iF_{base_case} represent *iF* calculated under sensitivity case and base-case assumptions, respectively.
[b] Population-weighted mean of sensitivity values over all cities.
[c] Population weighted 25th and 75th percentiles of sensitivity values over all cities

Table SI.5. Sensitivity of model results to other inputs. [a]

Model Parameter	Mean [b]	P_{25} [c]	P_{75} [c]
Aspect ratio (*L/W*, default = 1)			
α = 0.5	- 26%	- 28%	- 22%
α = 2	+ 33%	+ 26%	+ 38%
Breathing profile			
"Flat"	+ 13%	+ 5.2%	+ 22%
"Sine"	+ 16%	+ 11%	+ 21%
SoCAB-1	- 10%	- 13%	- 6.7%
SoCAB-2	+ 9.5%	+ 6.3%	+ 13%
Emissions Profile			
Flat	+ 1.0%	- 3.8%	+ 6.2%
Mexico	+ 1.8%	+ 0.9%	+ 2.7%
Delhi	+ 4.8%	+ 1.9%	+ 7.6%
Beijing	- 6.6%	- 9.1%	- 4.0%
USA NEI	-12%	-18%	-6.8%
Pollutant half-life (default: conserved)			
100 h	- 0.8%	- 1.6%	- 0.3%
10 h	- 7.2%	- 14%	- 2.6%

[a] Sensitivity is defined as $100 \times (iF_{sens\_case} - iF_{base\_case}) / iF_{base\_case}$, where iF_{sens_case} and iF_{base_case} represent *iF* calculated under sensitivity case and base-case assumptions, respectively.
[b] Population-weighted mean of sensitivity values over all cities.
[c] Population weighted 25th and 75th percentiles of sensitivity values over all cities

SI.2.2.2 – Influence of microenvironments

The single-compartment model employed here does not account for variability in exposure concentrations among microenvironments. Instead, we assume that the population-average exposure concentration attributable to vehicle emissions is reasonably approximated by the ambient (outdoor urban-average) vehicle-attributable concentration. Two prior studies of vehicle-associated population intake of conserved pollutants in Southern California found this assumption to be valid to within ± ~ 15-30%, depending on the pollutant under consideration.[10, 11] To further estimate the range of uncertainty associated with this assumption, we present here the results of a bounding analysis.

To estimate the error associated with neglecting variability in vehicle-attributable exposure concentrations among microenvironments, we introduce the sensitivity parameter ε, which represents the percentage difference between an *iF* estimated based on microenvironmental

concentrations and one estimated using a single ambient concentration. Neglecting differences in breathing rate among microenvironments, ε can be estimated as:

$$\varepsilon \sim 100 \times \left(\sum_{\mu=1}^{N} T_\mu \gamma_\mu - 1 \right) \quad \text{SI.4}$$

Here, for one of $\mu = 1 \ldots N$ microenvironments, T_μ represents the fraction of population-time spent in that microenvironment, and γ_μ represents the ratio between the vehicle attributable concentration in that microenvironment and in the overall urban (outdoor) environment. Following Marshall et al., we consider three microenvironments: indoors, in-vehicle/near-roadway, and outdoors (not-near roadways). The microenvironmental time distribution (T) is based on analysis of the US NHAPS dataset (Table SI.6).[7] Indoor microenvironments account for an average of ~21 h d^{-1} of population-time. Interestingly, a very similar microenvironmental time distribution was reported for the population of Hong Kong.[19] Distributions of γ_μ may vary as a function of pollutant dynamics and characteristics of the built environment. Indicative values of γ_μ are reported in Table SI.6 and described here. For non-reactive gaseous primary pollutants (e.g., CO, benzene), $\gamma_\mu = 1$ for indoor conditions.[10] In contrast, $PM_{2.5}$ of outdoor origin is partially removed in buildings via deposition and filtration. We consider a nominal value of $\gamma_\mu = 0.6$ for primary $PM_{2.5}$.[11, 20] Considering roadway/in-vehicle microenvironments, γ_μ is typically ~ 3-4 for primary pollutants of vehicular origin.[10, 11, 21] Finally, by definition, $\gamma_\mu = 1$ for the outdoor microenvironment. Two pollutant classes for γ_μ, listed as "conserved primary" and "primary $PM_{2.5}$" in Table SI.6, summarize the above data. Considering these two cases, vehicle-attributable intake may be ~16 % higher than predicted by the base-case single compartment model for nonreactive primary pollutants, and ~24% lower than base-case estimates for $PM_{2.5}$ (Table SI.7). We conclude that microenvironments are likely to contribute less than ~ 30% absolute uncertainty in our results.

Table SI.6. Parameter values for microenvironment sensitivity analysis.

	Microenvironment		
	Indoors	*Vehicle/road*	*Other outdoor*
Time distribution	T_μ (h d^{-1})		
(from NHAPS)	20.9	1.3	1.8
Pollutant class	γ_μ (-)		
conserved primary	1	4	1
primary $PM_{2.5}$	0.6	3	1

Table SI.7. Sensitivity (ε) of *iF* considering microenvironments, relative to base-case

Pollutant class	**Sensitivity** (ε)
conserved primary	+ 16%
primary $PM_{2.5}$	- 24%

SI.2.3 Additional figures and tables

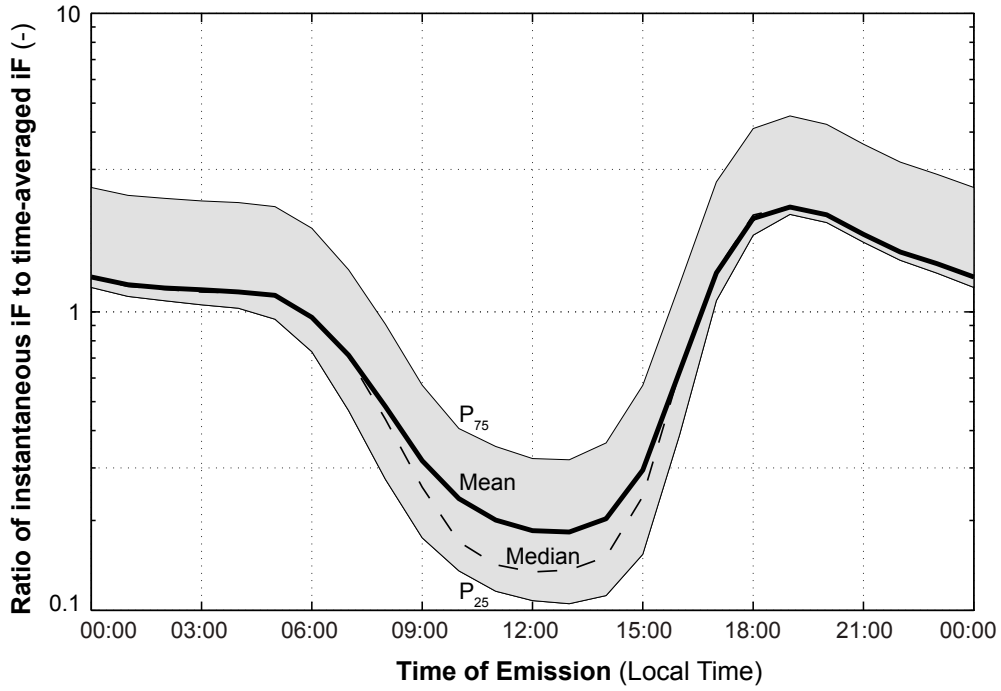

Figure SI.8. Variation in *iF* for emissions occurring at a specified time of day, expressed as a ratio of the time-dependent *iF* to time-averaged *iF* for a given city. Line marked "mean" represents the population-weighted mean value of this ratio for emissions at each hour of the day computed for 3646 cities. Similarly, lines marked median, P_{25} and P_{75} represent the median, 25th and 75th percentiles of the distribution of this ratio for each hour of emissions.

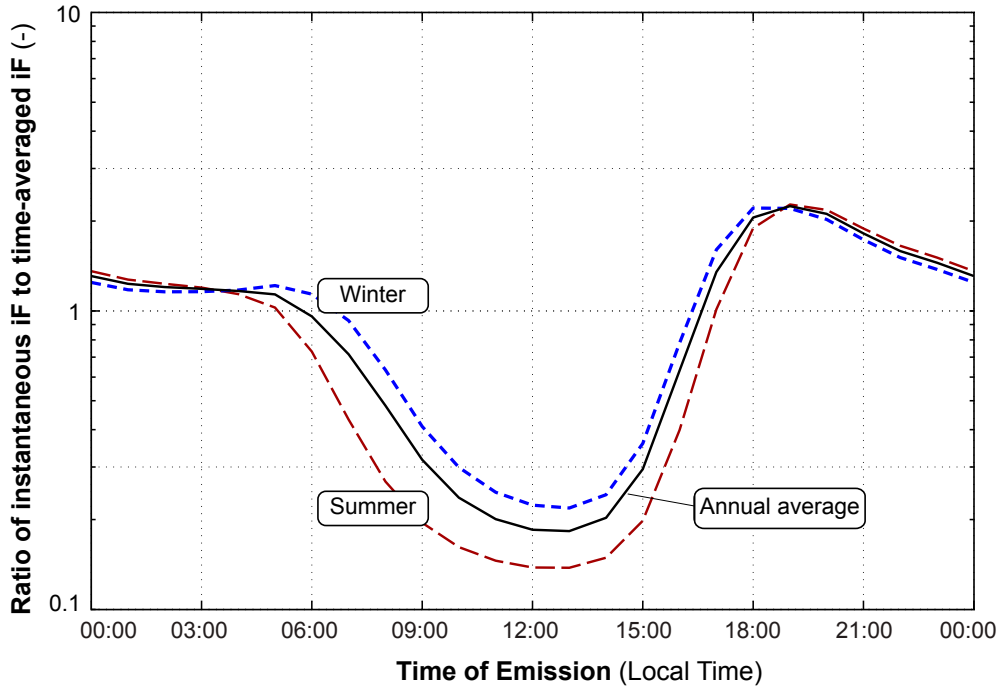

Figure SI.9. Seasonal variation in *iF* for emissions occurring at a specified time of day, expressed as a ratio of the time-dependent *iF* to time-averaged *iF* for a given city. Traces display the population-weighted mean value of this ratio for all non-tropical cities (absolute latitude > 23.5º; 2365 cities, 1.4 billion inhabitants). Line marked "annual average" displays the annual average of this ratio for emissions at a specific time of day. Winter trace represents emissions during Jan – Mar (cities in northern hemisphere) and Jul – Sep (southern hemisphere); summer trace represents emissions during Jul – Sep (northern hemisphere) and Jan – Mar (southern hemisphere).

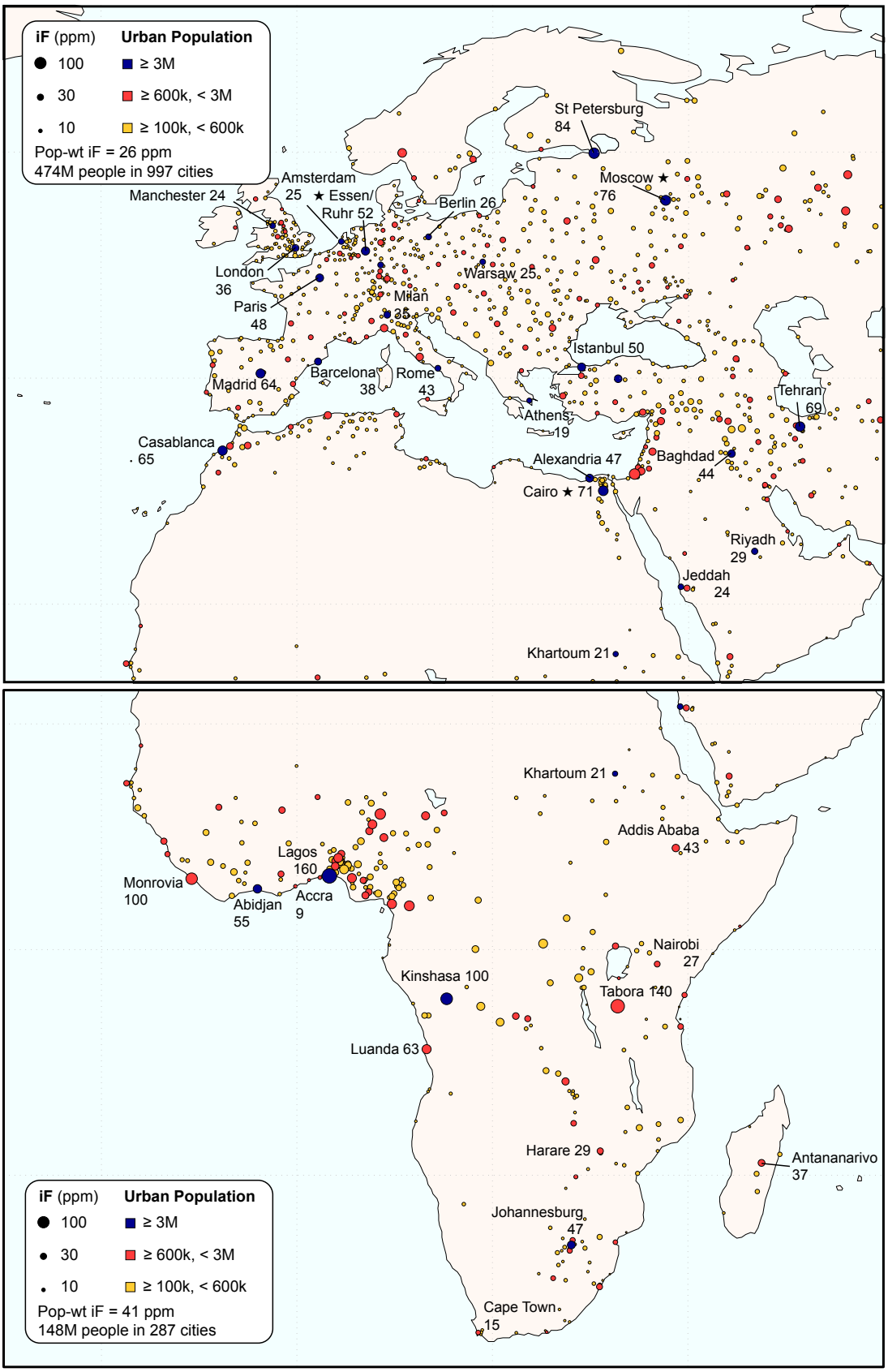

Figure SI.10a. Maps of *iF* results for Europe, Middle East, and Africa (cf. Fig 2)

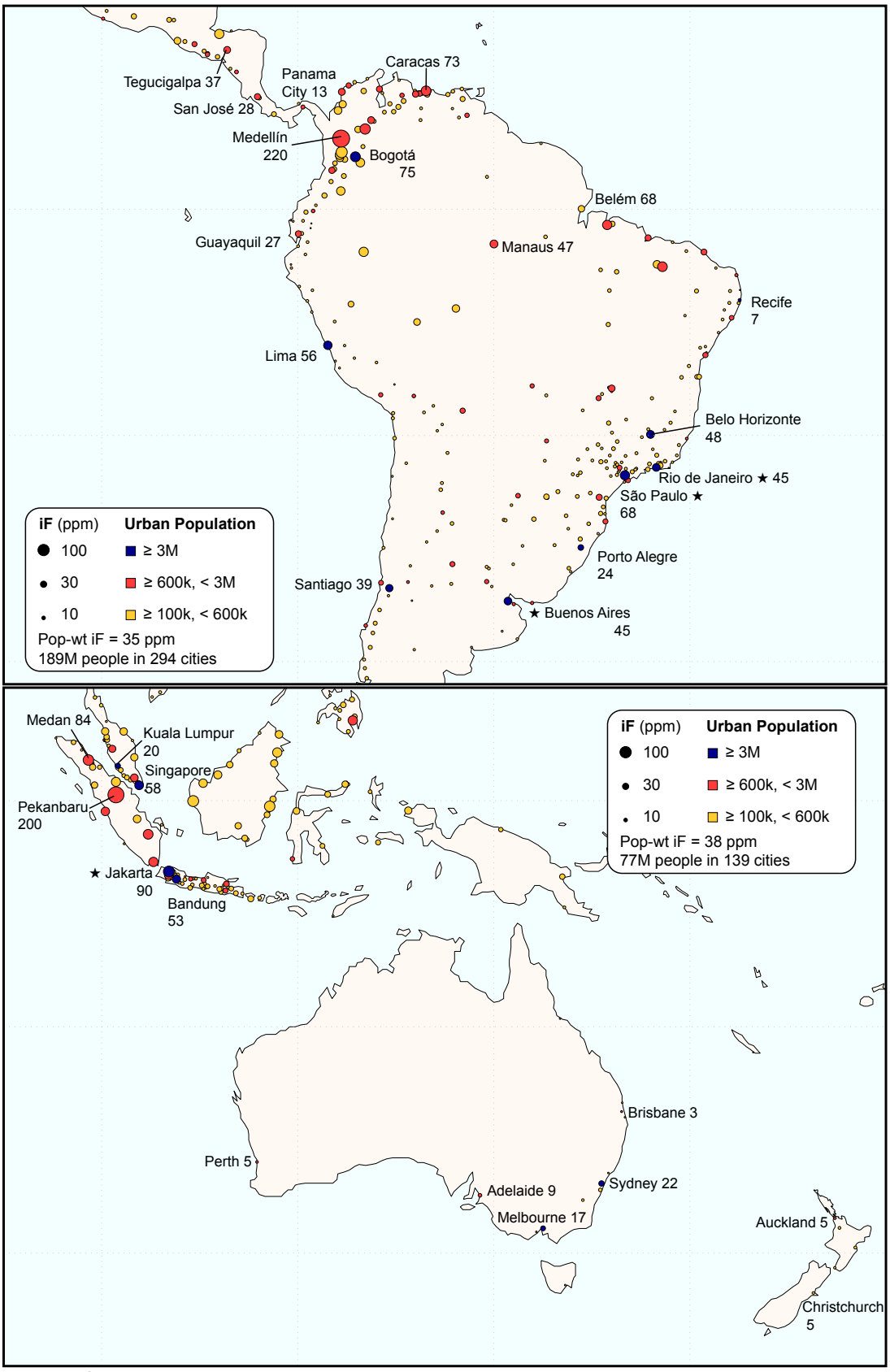

Figure SI.10b. Maps of *iF* results for Central and South America and Oceania (cf. Fig 2)

Table SI.8. Intake fraction results and summary data for 20 worldwide megacities

Megacity	Country	*iF* (ppm)	Population (millions)	*LPD* (population m^{-1})	*DR* (m^2 s^{-1})
Tokyo	Japan	94	34.5	524	489
New York [a]	USA	48	22.4	270	317
Mexico City	Mexico	145	18.4	520	224
Seoul	S. Korea	75	17.4	484	581
São Paulo	Brazil	68	17.1	369	467
Essen/Ruhr	Germany	52	16.9	291	527
Los Angeles [b]	USA	43	16.4	222	272
Mumbai	India	79	16.1	779	1200
Delhi	India	105	14.4	413	333
Shanghai	China	74	13.1	370	534
Kolkata	India	151	13.1	538	376
Osaka	Japan	25	13.0	300	1150
Buenos Aires	Argentina	45	12.6	295	601
Jakarta	Indonesia	90	11.0	315	307
Rio de Janeiro	Brazil	45	10.8	306	668
Beijing	China	73	10.8	317	383
Cairo	Egypt	71	10.4	400	556
Moscow	Russia	76	10.2	303	470
Dhaka	Bangladesh	262	10.1	715	297
Karachi	Pakistan	67	10.0	419	651

[a] New York includes New York City, Long Island, Northern New Jersey regions
[b] Los Angeles includes contiguous urban portions of Orange and Riverside counties

Table SI.9. Population-weighted mean intraurban *iF* for cities in all countries in dataset.

Country	Region	*iF* (ppm)	Cities	Pop (millions)
Afghanistan	SCA	49	12	4.4
Albania	EUJ	25	1	0.34
Algeria	NAF	20	33	8.3
Angola	SSA	53	5	3.1
Argentina	LAM	29	28	23
Armenia	WAS	17	3	1.4
Australia	LRD	14	13	13
Austria	EUJ	20	5	2.8
Azerbaijan	WAS	16	3	2.4
Bahamas, The	LAM	1.3	1	0.21
Bahrain	WAS	7	1	0.4
Bangladesh	SCA	190	20	18
Belarus	EUJ	19	15	4.7
Belgium	EUJ	13	11	5.3
Benin	SSA	11	3	1
Bolivia	LAM	12	7	3.6
Bosnia & Herzegovina	EUJ	24	2	0.56
Botswana	SSA	9.2	2	0.38
Brazil	LAM	33	130	88
Bulgaria	EUJ	14	9	2.6
Burkina Faso	SSA	27	2	1.4
Burundi	SSA	16	1	0.32
Cambodia	SEA	52	2	1.2
Cameroon	SSA	52	14	5.4
Canada	LRD	20	29	19
Central African Republic	SSA	30	1	0.58
Chad	SSA	23	2	0.75

Country	Region	*iF* (ppm)	Cities	Pop (millions)
Chile	LAM	27	18	9.4
China	EAP	44	830	410
Colombia	LAM	75	26	21
Congo, Democratic Republic	SSA	63	23	12
Congo, Republic	SSA	26	2	1.5
Costa Rica	LAM	27	2	1.1
Cote d'Ivoire	SSA	43	9	5.2
Croatia	EUJ	19	3	1
Cuba	LAM	16	12	4.4
Cyprus	WAS	4.8	2	0.37
Czech Republic	EUJ	11	6	2.2
Denmark	EUJ	7.7	4	1.6
Djibouti	SSA	12	1	0.46
Dominican Republic	LAM	25	8	3.1
Ecuador	LAM	15	14	5.4
Egypt	NAF	49	27	20
El Salvador	LAM	14	4	1.8
Eritrea	SSA	16	1	0.48
Estonia	EUJ	7.3	2	0.5
Ethiopia	SSA	36	6	3.3
Finland	EUJ	15	5	1.8
France	EUJ	25	50	27
Gabon	SSA	3.5	2	0.63
Gambia, The	SSA	9.1	1	0.32
Georgia	WAS	21	5	1.7
Germany	EUJ	30	73	49
Ghana	SSA	15	5	2.9
Greece	EUJ	17	6	4.6
Guatemala	LAM	19	2	1
Guinea	SSA	30	3	1.6
Guinea-Bissau	SSA	17	1	0.27
Haiti	LAM	30	2	1.9
Honduras	LAM	43	3	1.5
Hungary	EUJ	16	9	3
Iceland	EUJ	5.3	1	0.17
India	SCA	51	340	190
Indonesia	SEA	53	77	40
Iran	SCA	30	61	27
Iraq	WAS	29	22	14
Ireland	EUJ	8.7	2	1.2
Israel	WAS	23	8	4.6
Italy	EUJ	24	43	20
Jamaica	LAM	15	2	0.87
Japan	EUJ	50	100	85
Jordan	WAS	20	2	1.9
Kazakhstan	SCA	12	19	5.3
Kenya	SSA	23	5	3.6
Korea, Dem. Rep.	EAP	31	24	8.5
Korea, Rep.	EAP	46	33	36
Kosovo	EUJ	11	2	0.3
Kuwait	WAS	16	2	2.1
Kyrgyzstan	SCA	15	2	0.98
Laos	SEA	33	3	0.9
Latvia	EUJ	12	2	0.88
Lebanon	WAS	12	4	2.1
Liberia	SSA	100	1	0.69

Country	Region	*iF* (ppm)	Cities	Pop (millions)
Libya	NAF	10	14	4.7
Lithuania	EUJ	15	5	1.4
Macedonia	EUJ	17	2	0.6
Madagascar	SSA	29	6	2.1
Malawi	SSA	23	2	0.99
Malaysia	SEA	24	24	13
Mali	SSA	24	4	1.5
Mauritania	SSA	9.7	1	0.6
Mexico	LAM	65	82	58
Moldova	EUJ	13	4	1
Mongolia	EAP	21	1	0.76
Montenegro	EUJ	9.8	1	0.13
Morocco	NAF	35	20	11
Mozambique	SSA	15	9	2.7
Myanmar	SEA	45	15	6.5
Namibia	SSA	9.5	1	0.23
Nepal	SCA	30	4	1.1
Netherlands	EUJ	17	19	9.5
New Caledonia	EAP	0.8	1	0.13
New Zealand	LRD	4.6	6	2.3
Nicaragua	LAM	11	2	1.2
Niger	SSA	17	3	1.1
Nigeria	SSA	72	60	33
Norway	EUJ	39	5	1.4
Oman	WAS	10	3	0.98
Pakistan	SCA	47	56	34
Panama	LAM	13	3	1.2
Papua New Guinea	EAP	11	2	0.36
Paraguay	LAM	17	2	1.7
Peru	LAM	39	18	12
Philippines	SEA	44	31	18
Poland	EUJ	16	33	14
Portugal	EUJ	15	6	3.7
Puerto Rico	LAM	4.3	7	3.3
Qatar	WAS	6.2	1	0.5
Romania	EUJ	20	25	6.7
Russia	EUJ	32	160	68
Rwanda	SSA	30	1	0.52
Saudi Arabia	WAS	20	21	15
Senegal	SSA	21	7	2.9
Serbia	EUJ	19	5	1.7
Sierra Leone	SSA	20	3	1
Singapore	SEA	58	1	4.1
Slovakia	EUJ	11	2	0.69
Slovenia	EUJ	16	2	0.39
Somalia	SSA	6.9	7	2.3
South Africa	SSA	27	37	23
Spain	EUJ	31	43	20
Sri Lanka	SCA	12	4	1.5
Sudan	NAF	16	14	6.8
Suriname	LAM	4.3	1	0.23
Sweden	EUJ	22	10	3.2
Switzerland	EUJ	15	10	3.4
Syria	WAS	32	10	6.7
Tajikistan	SCA	12	2	0.71
Tanzania	SSA	46	13	6.9
Thailand	SEA	33	17	9.8

Country	Region	*iF* (ppm)	Cities	Pop (millions)
Togo	SSA	7.7	1	0.73
Tunisia	NAF	17	6	2.6
Turkey	WAS	31	55	29
Turkmenistan	SCA	11	5	1.3
Uganda	SSA	31	1	1.1
Ukraine	EUJ	15	45	18
United Arab Emirates	WAS	9.5	4	2.4
United Kingdom	EUJ	19	66	32
United States	LRD	21	240	190
Uruguay	LAM	8.6	1	1.3
Uzbekistan	SCA	14	17	5.5
Venezuela	LAM	30	31	14
Vietnam	SEA	71	26	14
West Bank & Gaza	WAS	69	4	1.9
Western Sahara	NAF	5	1	0.17
Yemen	WAS	19	7	3
Zambia	SSA	18	7	2.6
Zimbabwe	SSA	21	5	2.7

References

1. Hanna, S. R.; Briggs, G. A.; Hosker, R. P., Jr. *Handbook on Atmospheric Diffusion*; DOE/TIC-112233; Office of Energy Research, US Department of Energy: Washington, DC, 1982; http://www.orau.org/ptp/PTP Library/library/Subject/Meteorology/handbook on atmospheric diffusion.pdf.
2. Stevens, G.; de Foy, B.; West, J. J.; Levy, J. I. Developing intake fraction estimates with limited data: Comparison of methods in Mexico City. *Atmos. Environ.* **2007**, *41*, 3672-3683.
3. Seinfeld, J. H.; Pandis, S. N., *Atmospheric Chemistry and Physics, Second Edition: From Air Pollution to Climate Change*. Wiley-Interscience: Hoboken, NJ, 2006.
4. Heath, G. A. Redistributing pollution: Exposure implications of a shift toward distributed electricity generation in California. PhD Dissertation, University of California, Berkeley, 2006.
5. Irwin, J. S. A theoretical variation of the wind profile power-law exponent as a function of surface roughness and stability. *Atmos. Environ.* **1979**, *13*, 191-194.
6. *Metabolically Derived Human Ventilation Rates: A Revised Approach Based Upon Oxygen Consumption Rates*; EPA/600/R-06/129F; United States Environmental Protection Agency, National Center for Environmental Assessment: Washington, DC, 2009; http://cfpub.epa.gov/ncea/cfm/recordisplay.cfm?deid=202543.
7. Klepeis, N. E.; Nelson, W. C.; Ott, W. R.; Robinson, J. P.; Tsang, A. M.; Switzer, P.; Behar, J. V.; Hern, S. C.; Engelmann, W. H. The National Human Activity Pattern Survey (NHAPS): a resource for assessing exposure to environmental pollutants. *J. Exposure Anal. Environ. Epidemiol.* **2001**, *11*, 231-252.
8. *Exposure Factors Handbook: 2009 Update (External Review Draft)*; EPA/600/R-09/052A; US Environmental Protection Agency: Washington, DC, 2009; http://cfpub.epa.gov/ncea/cfm/recordisplay.cfm?deid=209866.

9. Stephenson, R.; Mohan, R. M.; Duffin, J.; Jarsky, T. M. Circadian rhythms in the chemoreflex control of breathing. *Am. J. Physiol.-Reg. I.* **2000**, *278*, R282-R286.
10. Marshall, J. D.; Riley, W. J.; McKone, T. E.; Nazaroff, W. W. Intake fraction of primary pollutants: motor vehicle emissions in the South Coast Air Basin. *Atmos. Environ.* **2003**, *37*, 3455-3468.
11. Marshall, J. D.; Granvold, P. W.; Hoats, A. S.; McKone, T. E.; Deakin, E.; Nazaroff, W. W. Inhalation intake of ambient air pollution in California's South Coast Air Basin. *Atmos. Environ.* **2006**, *40*, 4381-4392.
12. Sathaye, N.; Harley, R.; Madanat, S. Unintended environmental impacts of nighttime freight logistics activities. *Transp. Res. A* **2010**, *44*, 642-659.
13. Westerdahl, D.; Wang, X.; Pan, X.; Zhang, K. M. Characterization of on-road vehicle emission factors and microenvironmental air quality in Beijing, China. *Atmos. Environ.* **2009**, *43*, 697-705.
14. Guttikunda, S. K., Personal communication: diurnal profiles for Delhi emissions inventory. June 8, 2011.
15. Huo, H.; Zhang, Q.; He, K.; Wang, Q.; Yao, Z.; Streets, D. G. High-resolution vehicular emission inventory using a link-based method: a case study of light-duty vehicles in Beijing. *Environ. Sci. Technol.* **2009**, *43*, 2394-2399.
16. *The National Emissions Inventory*; United States Environmental Protection Agency: Washington, DC, 2011; http://www.epa.gov/ttn/chief/net/2008inventory.html.
17. Angel, S.; Parent, J.; Civco, D.; Blei, A.; Potere, D. *A Planet of Cities: Urban Land Cover Estimates and Projections for All Countries, 2000-2050*; WP10SA3; Lincoln Institute of Land Policy: Cambridge, MA, 2010; http://www.lincolninst.edu/pubs/1861_A-Planet-of-Cities.
18. Angel, S.; Parent, J.; Civco, D. L.; Blei, A.; Potere, D. The dimensions of global urban expansion: Estimates and projections for all countries, 2000-2050. *Prog. Plann.* **2011**, *75*, 53-107.
19. Luo, Z.; Li, Y.; Nazaroff, W. W. Intake fraction of nonreactive motor vehicle exhaust in Hong Kong. *Atmos. Environ.* **2010**, *44*, 1913-1918.
20. Riley, W. J.; McKone, T. E.; Lai, A. C. K.; Nazaroff, W. W. Indoor particulate matter of outdoor origin: Importance of size-dependent removal mechanisms. *Environ. Sci. Technol.* **2002**, *36*, 200-207.
21. Apte, J. S.; Kirchstetter, T. W.; Reich, A. H.; Deshpande, S. J.; Kaushik, G.; Chel, A.; Marshall, J. D.; Nazaroff, W. W. Concentrations of fine, ultrafine, and black carbon particles in auto-rickshaws in New Delhi, India. *Atmos. Environ.* **2011**, *45*, 4470-4480.